Recent Developments in Optical and Thermal Performance of Direct Absorption Solar Collectors

Muzamil Hussain [1], Syed Khawar Hussain Shah [1], Uzair Sajjad [2], Naseem Abbas [3,*] and Ahsan Ali [4,*]

1   Department of Mechanical Engineering, COMSATS University Islamabad, Sahiwal Campus,
    Sahiwal 57000, Pakistan
2   Department of Energy and Refrigerating Air-Conditioning Engineering, National Taipei University of
    Technology, Taipei 10608, Taiwan
3   Department of Mechanical Engineering, Sejong University, Seoul 05006, Korea
4   Department of Mechanical Engineering, Gachon University, Seongnam-si 13120, Korea
*   Correspondence: naseem.abbas@sejong.ac.kr (N.A.); ahsanali@gachon.ac.kr (A.A.)

Abstract: Solar energy is the most promising green energy resource, as there is an enormous supply of solar power. It is considered a good potential solution for energy crises in both domestic and industrial sectors. Nowadays, many types of solar systems are used for harvesting solar energy. Most of the research is focused on direct absorption solar collectors (DASCs) due to their ability to capture more solar energy. The effectiveness of DASCs is dependent on various factors, such as working fluid properties, geometry, and operating parameters. This review summarizes the impact of different design and operating parameters on the performance of DASCs. Many effective parameters are considered and their impact on optical and thermal properties is summarized. The influence of working fluid parameters, such as base fluid type, nanoparticle type, nanoparticle size, nanoparticle shape, and nanoparticle concentration on heat transfer performance, was discussed and their optimum range was suggested. The effects of collector dimensions and many novel design configurations were discussed. The effect of the most important operating parameters, such as temperature, flow rate, flow regime, and irradiance on collector performance, was briefly summarized.

Keywords: solar energy; direct absorption solar collector; working fluid

1. Introduction

Today's world is striving for green energy resources to support sustainable living on planet Earth. Renewable energy resources are considered to be a solution to the problem, and solar energy is a potential candidate to cope with energy crisis as compared to others, due to low maintenance cost and the enormous supply of solar power from the sun. The effectiveness of a solar panel is dependent on various factors, such as its geometry, photothermal to photovoltaic conversion, and its position relative to sun rays.

The efficacy of a photovoltaic system is very much dependent on the working fluid and its thermal characteristics. Normally, water is used in this kind of system, but it is not an efficient working fluid due to its inadequate thermophysical properties. There is a need for such working fluids which are more efficient in terms of their thermophysical properties. Researchers have tested nanofluids in solar applications and a significant increase in photothermal efficiency has been witnessed [1]. In order to evaluate the performance of nanofluids as a working fluid, multiple studies have been carried out, in which different relationships have been proposed to estimate the thermophysical properties of nanofluids. Despite the suitable properties of nanofluids, their dispersion stability is a key challenge for utilizing these in solar collectors. The nanofluid stability is directly associated with thermal and optical properties of the solar system [2–5].

Solar radiation is converted into thermal energy in a solar system with the help of a working fluid [6]. The performance of a solar collector depends on design parameters and working fluids [7,8]. The geometry of a solar collector is modified to optimize the optical absorption and heat transfer performance of a working fluid, and to minimize heat losses [9–11]. Nowadays, many types of solar systems, such as Flat Plate Solar Collectors (FPSC), Parabolic Trough Solar Collectors (PTSC), Evacuated Tube Solar Collectors (ETSC), Photovoltaic Thermal Systems (PV/T), and Direct Absorption Solar Collectors (DASC) are used for harvesting solar energy. Of all the solar systems, more researchers are working on DASC due to its ability to capture more heat as compared to the others [12]. The solar radiation in a DASC is absorbed by working fluid within a transparent enclosed medium [13]. This solar collector gently absorbs the solar radiation to heat the working fluid and not the surface, reducing thermal losses and increasing thermal yield [14].

The quantity of solar irradiance absorbed by working fluids relies on different factors, such as working fluid properties, fluid category, and geometry of the receiver. Nanoparticles act as a booster when added to a working fluid and improve the absorption attributes of the working fluid [15]. Most of the solar radiations are absorbed by the scattered nanoparticles in the working fluid; only a small amount is lost during transmission through the glass of the panel [16]. DASCs incorporated with nanofluids are proposed to enhance the performance of photovoltaic systems. In order to further enhance the efficacy of solar systems, nanofluids-based DASCs are proposed by different researchers [17–19].

It is understood from the work of different researchers that design modification in solar systems enhances their performance. Several investigations have been carried out to look into the effect of nanoparticle size, shape, and concentration on the thermal efficiencies of the solar system [20–23]. As compared to surface absorption collectors, a DASC with hybrid nanofluid is a more efficient system due to the greater number of nanoparticles in bulk fluid volume, which results in negligible loss of heat to the environment, hence increasing the system performance. Moreover, the increased stability and optical characteristics, in addition to the reduced erosion, improve the efficiency of hybrid nanofluids in DASCs.

In this review, the impact of many factors on the performance of DASC is discussed. Many effective parameters are considered and their impact on optical and thermal properties is summarized. This review will help to develop the optimized DASC model based on selected parameters.

2. Working Fluid Properties

Thermophysical properties and heat transfer capability of a base fluid are affected by different factors, some of them being the type of nanoparticle, working fluid type, nanoparticle size, and the shape and concentration of nanoparticles in the working fluid. The most important factors are briefly described below.

2.1. Base Fluid Type

The efficacy of a thermal system is greatly influenced by the thermophysical properties of the working fluid [24]. Various types of base fluids are commonly used in solar systems. Examples of these are water, thermal oils, paraffin oil, Ethylene Glycol (EG), etc. The thermal efficacy of solar systems is dependent on the absorption properties of base fluid [25]. It is found that when nanoparticles are mixed in the neutral base fluid, the base fluid depicts optimum thermophysical properties in terms of viscosity, thermal conductivity, and heat transfer in comparison to other base fluids [26]. Menni et al. [27] performed a numerical study to compare the thermal and hydrodynamic properties of different base fluids, including water, ethylene glycol, and ethylene glycol-water mixture, by dispersing the Al2O3 nanoparticles. The results of the numerical study showed that ethylene glycol shows superior thermophysical properties as compared to the other two base fluids. The results showed that the Nusselt numbers of pure ethylene glycol and ethylene glycol-based nanofluids are higher at all ranges of the Reynolds number as compared to water and mixture-based nanofluids. However, the variation in the friction coefficient

is negligible, and all base fluids and nanofluids exhibit approximate the same values of friction coefficients.

Gholinia et al. [28] worked on water, engine oil, and ethylene glycol by dispersing carbon nanoparticles. The results showed that the engine oil shows superior temperature and flow characteristics as compared to water. Gao et al. [29] analyzed the ethylene glycol and water base fluids using a graphene nanoplatelet (GNP). The highest values of thermal conductivity were recorded for a blend of water and ethylene glycol in a ratio of 1:1. Ethylene glycol exhibits a higher thermal conductivity when blended with water. Cao et al. [30] investigated whether the presence of anion and cation radii in base working fluids is effective to enhance the absorption characteristics of base fluids for DASCs. The literature showed that ethylene glycol has superior thermal properties in DASCs as compared to water, and engine oil also has superior thermal properties as compared to water. Moreover, the blend of ethylene glycol and water can be used to enhance thermal properties.

2.2. Nanoparticles Type

Many metal-based nanoparticles, such as Al, Cu, Ag, Au, Al_2O_3, CuO, ZnO, MgO, Fe_3O_4, TiO_2, etc., and carbon-based nanoparticles such as carbon nanotubes (CNTs), graphene, etc., have been used for making the working fluids by dispersing these nanoparticles in base fluids [31–33]. Wang et al. [34] tested the DASC using a suspension of graphene and MXene nanoparticles as a working fluid. Both graphene and MXene nanofluids were compared in terms of thermal conductivity at different temperatures and concentrations of graphene and MXene nanoparticles. The results obtained are presented in Figure 1. The results presented showed that the graphene nanofluids exhibit values of thermal conductivity compared to MXene at all concentrations and temperatures. Vakili et al. [35] prepared the nanofluid using graphene nanoplatelets and investigated the performance of the DASC using this nanofluid. The performance of the DASC operated with graphene nanofluids was found to be higher as compared to the DASC operated using water, under the same operating conditions.
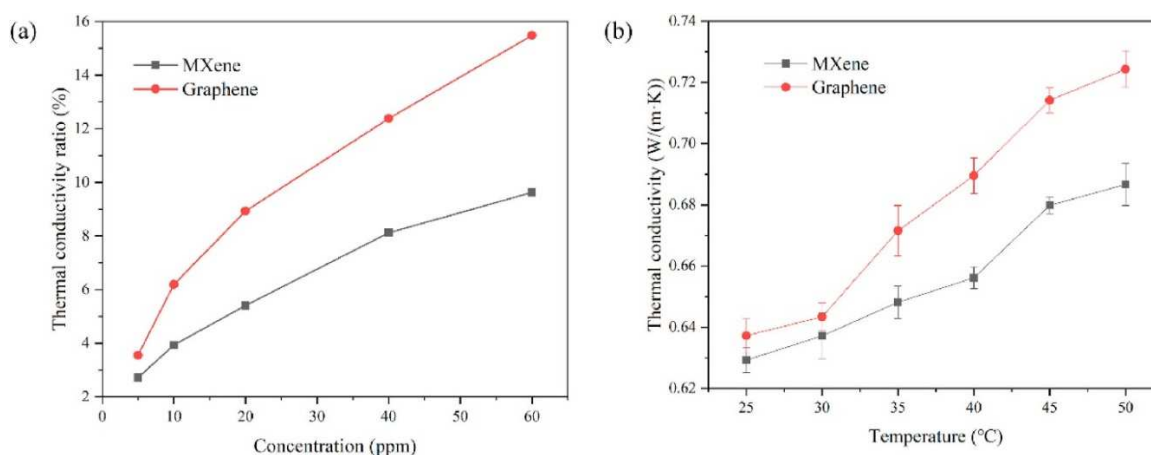

Figure 1. Thermal conductivity of MXene and Graphene nanofluids. (**a**) Thermal conductivity vs. nanoparticle concentration at 45 °C. (**b**) Thermal conductivity vs. temperature. Modified and printed with permission from [34].

Zheng et al. [36] prepared the water-based mono multi-walled carbon nanotubes (MWCNT) and hybrid MWCNT-TiN nanofluids, and used these nanofluids in DASCs to improve the optical characteristics of working fluids as compared to conventional working fluids. The highest solar absorption and photothermal conversion capabilities were observed for MWCNT nanofluids at a 10 ppm concentration of MWCNT nanoparticles. The solar absorption characteristics of nanofluids were further improved by the addition of TiN nanoparticles in suspensions up to a mass fraction of 10 ppm. Joseph et al. [37] analyzed the effect of C-dot/water nanofluids on the performance of the DASC. Approximately

five times the solar collector efficiency of the DASC was recorded as compared to water, due to the application of C-dot/water nanofluid. Kumar et al. [38] added porous carbon nanoparticles to the base fluid and analyzed the performance of the DASC system. The enhancement in solar absorption efficiency was observed using a porous activated carbon nanofluid. Highly stable low-cost porous carbon nanofluid was found suitable for use in DASC systems. Hazara et al. [39] found that the addition of carbon nanoparticles in working fluid is beneficial for improving the solar absorption capability of DASCs.

The literature depicted that metal-based nanofluids show better thermal performance due to their high conductivity [40–43]. Some studies showed that TiN nanofluids have superior photothermal and optical characteristics, and can be used in DASCs as a working fluid [44]. The literature exhibited that the dispersion of carbon-based nanoparticles in base fluids is more effective for enhancing the thermal properties as compared to other types of nanoparticles [45–48].

2.3. Particle Size

Many authors examined the influence of nanoparticle size on the performance of DASCs. Said et al. [49] studied the effect of TiO_2 nanoparticle size on optical characteristics in DASCs. The results showed that smaller nanoparticle size (<20 nm) is beneficial for improving the optical characteristics of nanofluids. The results of the study are presented in Figure 2a, which shows that particle size has no significant influence on the extinction coefficient. The 0% transmissivity was observed for a particle size of 20 nm within the 200–300 nm wavelength range, as shown in Figure 2b. However, a sudden surge was detected in transmissivity when the wavelength reached 400 nm.
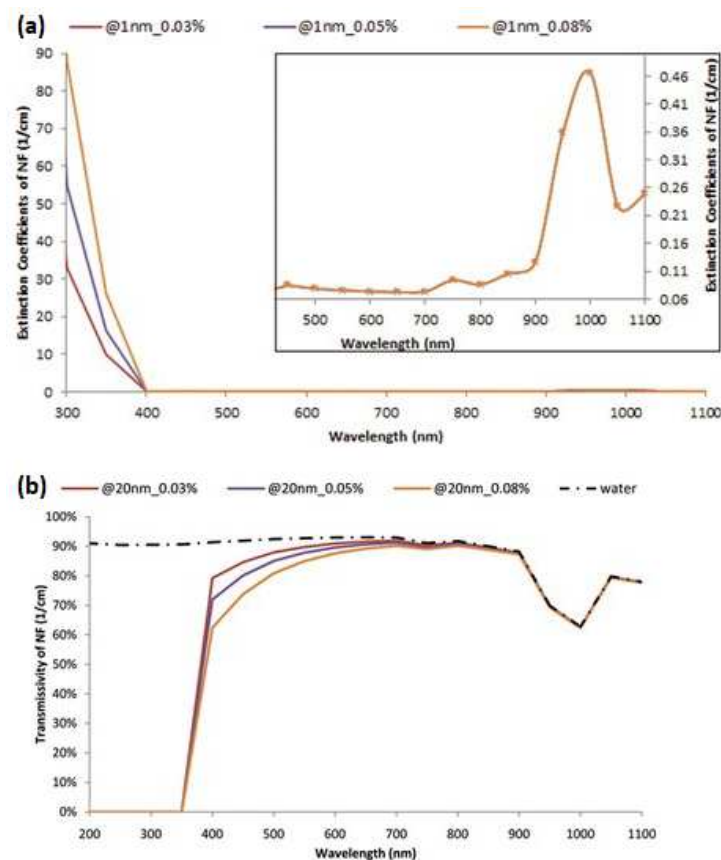

Figure 2. Influence of nanoparticle size on optical characteristics. (**a**) Influence of nanoparticle size on extinction coefficient. (**b**) Influence of nanoparticle size on transmissivity. Modified and printed with permission from [49].

Howe et al. [50] worked on the consequences of size, concentration, and shape of the nanoparticle on optical properties of nanofluids. Smaller-sized nanoparticles exhibit less transmittance and absorb light in better ways. Rod type nanoparticles exhibit higher transmittance and absorb less light. The results are presented in Figure 3.
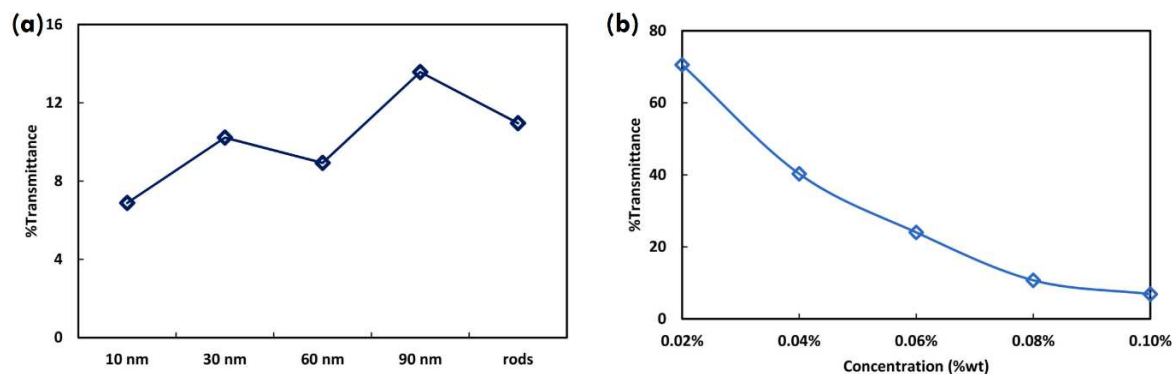

Figure 3. Effect of nanoparticle size, shape, and concentration on transmittance. (**a**) Effect of size and shape. (**b**) Effect of concentration. Modified and printed with permission from [50].

The particle scattering is normally neglected in the DASC by assuming a smaller nanoparticle size than the radiation wavelength [22–25]. The practice of neglecting the scattering effect is justifiable in near-infrared and visible regimes; however, the scattering becomes reasonable when a localized surface plasmon effect is produced as a result of metallic nanoparticle excitation [15]. The scattering effect of the nanoparticle cannot be neglected for a higher particle size. Therefore, the light scattering from particle excitation must be considered for thermal analysis. Won et al. [16] studied the influence of nanoparticle size on optical chrematistics in DASCs. The silica-gold nanoparticles of different thicknesses and radii were used for making nanofluids, and the effect of light scattering was studied. The results are presented in Figure 4. The results showed that the scattering efficiency was much less than the absorption efficiency for a 10 nm thickness and radius of core–shell particle (Figure 4a). However, the scattering efficiency was much higher than the absorption efficiency for a 10 nm shell thickness and 80 nm core radius of the core–shell particle (Figure 4b). Moreover, the resonance of the surface plasmon varied with the geometry and size of the nanoparticle.

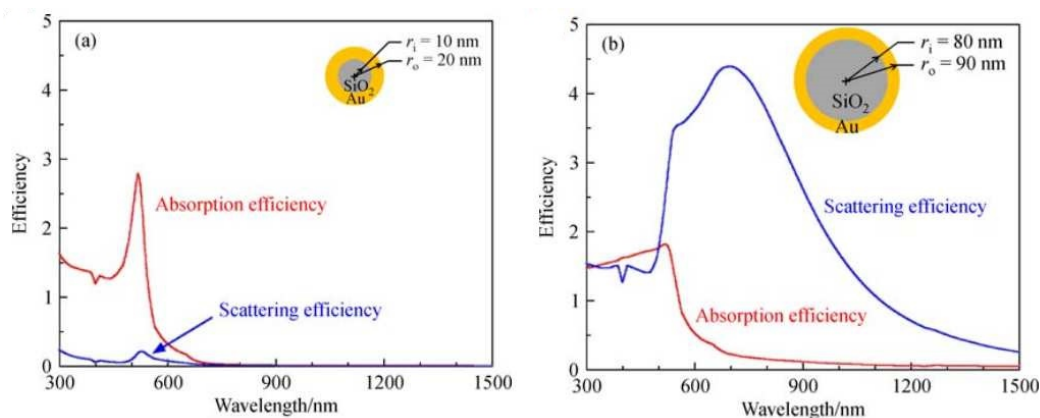**Figure 4.** Optical characteristics of silica-gold nano core–shell. (**a**) Silica radius of 10 nm and gold thickness of 10 nm. (**b**) Silica radius of 80 nm and gold thickness of 10 nm. Modified and printed with permission from [16].

It is suggested that the size of nanoparticles in the base fluid must be smaller for the purpose of achieving better thermophysical properties of working fluids in solar collec-

tors [51]. Moreover, the light scattering effect can be avoided by reducing the particle size. Therefore, the nanoparticle size must be smaller in order to achieve the optimum optical and thermophysical properties [52]. At elevated temperatures and higher concentrations of nanoparticles, this trend is converges more often [53–55]. A negligible increase in thermal conductivity has been noticed for large-sized nanoparticles. Heat transfer augments with the fluid layer around the nanoparticles in a nanofluid. By enhancing the size of nanoparticles, fluid layer thickness also increases, which results in enhanced thermal conductivity of working fluid.

2.4. Particle Shape

The variation in particle geometry led to the change in nanofluid properties, due to the change in reaction behavior between the nanoparticle and base fluid [56]. The absorption capability of a nanoparticle can be improved by altering the shape of the nanoparticle. Qin et al. [57] developed the sharp-edged Ag nanoparticles (i.e., with a smaller angle of edges and radius of curvature) to make these capable of inducing several absorption peaks at various wavelengths. The multiple absorption peaks were achieved due to the lightning rod and surface plasmon effect of Ag sharp-edged nanoparticles. Further, the absorption band was expanded by developing the SiO_2/Ag core–shell configuration. A 35% enhancement in the solar absorption coefficient was recorded for four-edged Ag nanospheres, while 20% enhancement was recorded for four-edged Ag nanorods as compared to single-edged Ag nanoparticles. The results are presented in Figure 5.
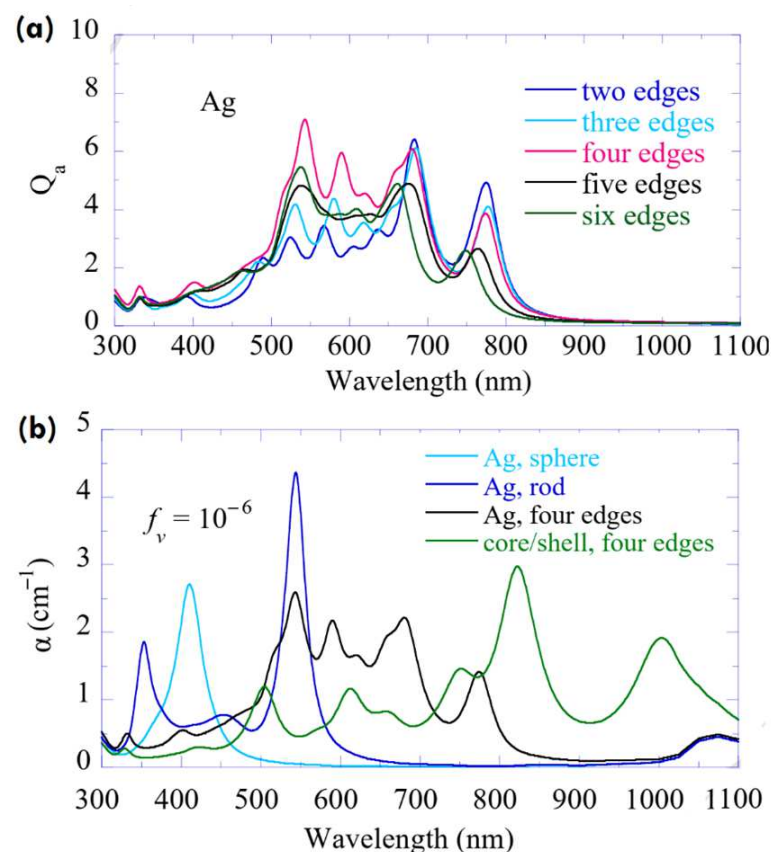
Figure 5. Influence of particle shape on absorption characteristics of working fluid in the DASC. (**a**) Solar absorption efficiency of nanofluids with different sharp edges. (**b**) Absorption coefficient of different nanofluids (made of Ag nanorod, Ag nanosphere, four-edged Ag nanoparticle, and four-edged SiO_2/Ag core–shell) at the same particle concentration and operating conditions. Modified and printed with permission from [57].

Compos et al. [23] studied the influence of particle shape on the photothermal efficiency of a DASC. The spherical and non-spherical nanoparticles of different metals, including silver, gold, and copper, were used for the production of different nanofluids. The comparison of DASC performance using spherical and cubic silver nanofluids is presented in Figure 6. The results show that the nanofluid prepared from cubic silver nanoparticles exhibited higher performance as compared to the nanofluid prepared from the spherical nanoparticles. The results of temperature and photothermal efficiency are presented in Figure 6a,b respectively.
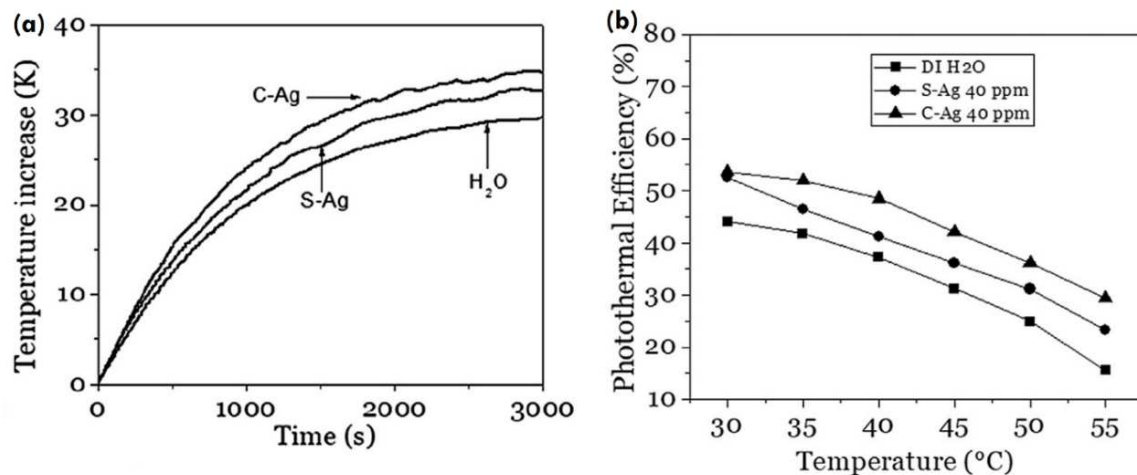

Figure 6. Influence of particle shape on thermal characteristics of a DASC. (**a**) Rise in temperature at different time intervals for spherical and cubic silver nanofluid. (**b**) Photothermal efficiency at different temperatures for spherical and cubic silver nanofluid. Modified and printed with permission from [23].

The literature shows that the nanofluids made of sharp-edged or cubic particles exhibit higher absorption properties and thermal conductivity as compared to spherical or rod-shaped nanoparticles [54,58]. The platelet-shaped or cylindrical particles induce higher performance in terms of entropy and viscosity generation and thermal conductivity [59–63]. Moreover, the nanoparticles with anisotropic characteristics and multiple surfaces show higher absorption and thermal properties.

2.5. Particle Concentraion

It has been found that within a certain limit of a particle concentration, the thermal properties of nanofluids are increased; beyond the limit, thermal conductivity begins to decrease due to the clustering effect. At higher volume fractions, the viscosity is increased due to the increase in non-Newtonian behavior [64–70]. However, the pumping power is increased due to an increase in viscosity [71,72]. It is concluded by many authors that the volume fraction up to 1 wt.% is effective, and beyond this, the performance of nanofluid is decreased. The particle–particle and particle–wall interactions are dependent on particle concentration [73,74].

Bardsgard et al. [13] used the Eulerian model to optimize different parameters, such as particle concentration and collector height for the DASC. The extinction coefficients of different particle concentrations were presented. The maximum efficiency of a DASC was achieved on 0.3 wt.% particle concentration and a decrease in efficiency was observed for more than 0.5 wt.% concentration. The maximum efficiency (68%) of a collector was achieved for the 300 μm thickness of the receiver. The effect of particle concentration on extinction coefficients and collector efficiency is presented in Figure 7.
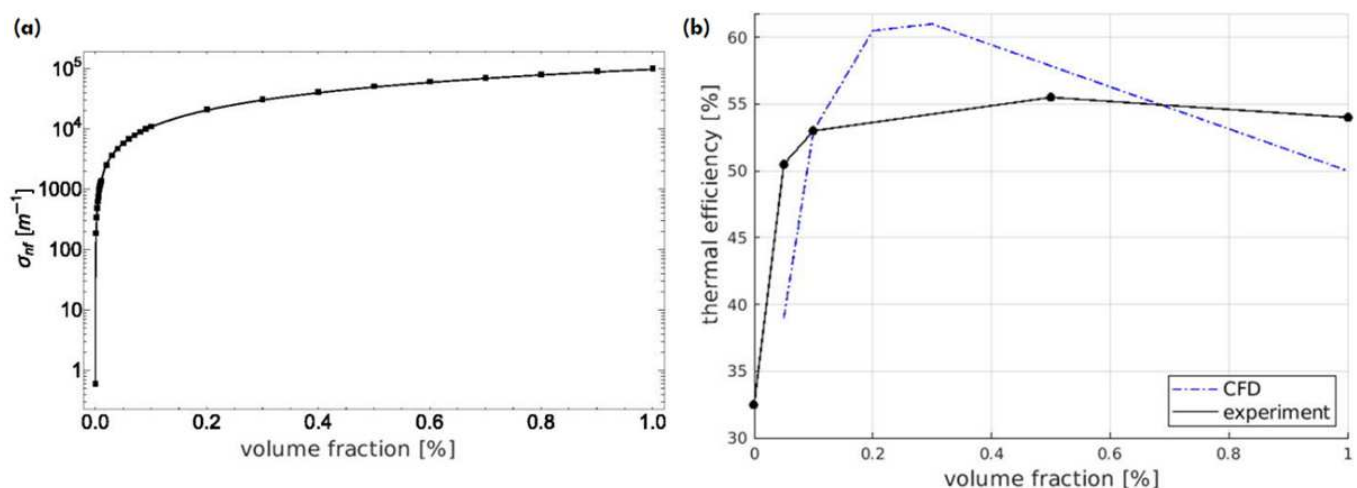
Figure 7. Effect of particle concentration on the optical and thermal performance of a collector. (**a**) Trend of extinction coefficients versus volume fraction. (**b**) Trend of collector efficiency versus volume fraction. Modified and printed with permission from [13].

3. Geometrical Parameters

The performance of a solar system depends on various parameters, such as the type of solar system and geometrical parameters of the collector.

3.1. Collector Length

It is observed that collector efficiency changes with the change in length. Initially, it starts improving by increasing the length; later, it starts decreasing. By increasing the length of the collector, the surface area of the collector also increases, which helps solar panels to capture more solar radiation. However, it was observed that after a certain limit, the performance of the solar panel deteriorates, which results in heat loss. Due to the increased surface area, working fluid is exposed to radiation for more time, which leads to increased outlet temperature. Sharaf et al. [75] utilized energy and exergy analysis to optimize the performance of the DASC. During experimentation it was found that exergy efficiency is enhanced with an increase in collector length up to an extent, after which it begins reducing. In order to gain the most useful power, an appropriate fluid velocity according to the collector length must be selected.

3.2. Collector Depth

Collector depth also influences the efficiency of solar panels. With the increase of collector depth, the efficiency of the solar panels is also enhanced, as working fluid can absorb more solar radiation. Radiative transfer equations coupled with conduction and convection heat transfer equations are utilized by Gorji and Ranjbar [76] for evaluating the effect of collector geometry on the performance of the DASC with nanofluid. A significant enhancement in collector efficiency was observed by increasing the depth of the collector. Vital et al. [77] studied the effect of collector thickness on collector thermal efficiency of a DASC. The results of the study are presented in Figure 8. The results showed that the thermal efficiency of a DASC increases with an increase in the collector thickness. The maximum performance was reached for H > 3. Bardsgard et al. [13] used the Eulerian model to optimize the different parameters such as particle concentration, and collector height for the DASC. The maximum efficiency (68%) of a collector was achieved for the 300 μm thickness of the receiver.
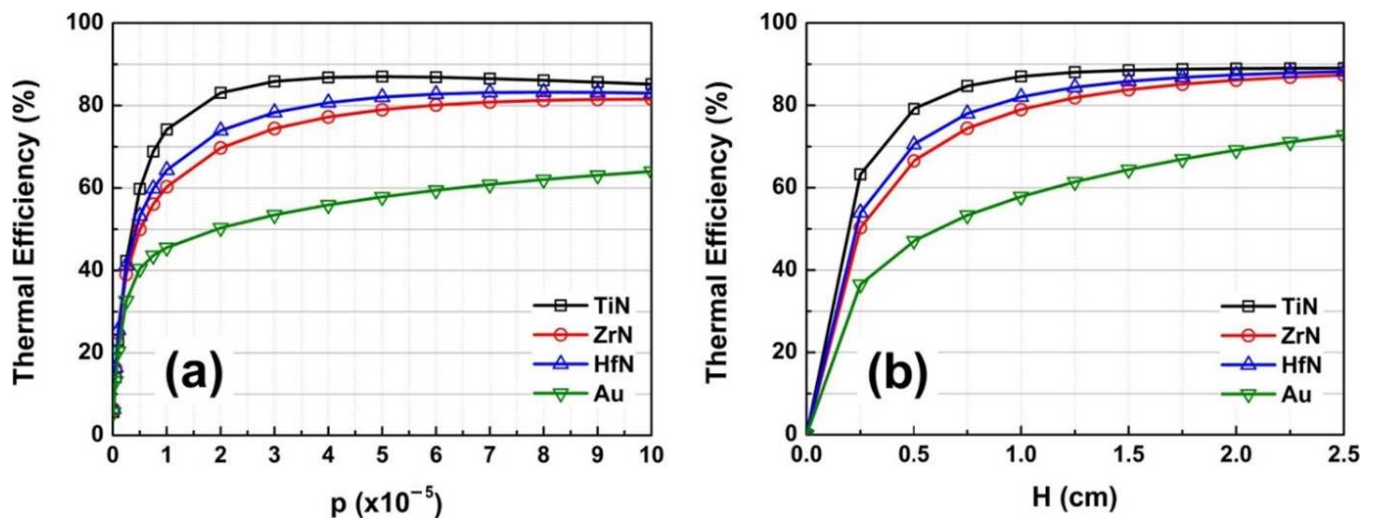
Figure 8. Thermal efficiency of a DASC operating with different nanofluids. (**a**) Thermal efficiency vs. nanoparticle concentration for collector thickness of 1 cm. (**b**) Thermal efficiency vs. collector thickness. Modified and printed with permission from [77].

3.3. Collector Design

Struchalin et al. [78] showed that a tabular DASC working with nanofluids is more efficient than a conventional DASC. They compared the thermal efficiency of a tabular DASC with commercial and flat plate collectors. They demonstrated that the tabular DASC exhibited a 20 to 25% higher efficiency as compared to vacuum tube type and flat plate type collectors. The results of the study are shown in Figure 9. In another study [79], they tested the tabular DASC system using magnetic Fe_3O_4 nanofluids and multi-walled carbon nanotubes.
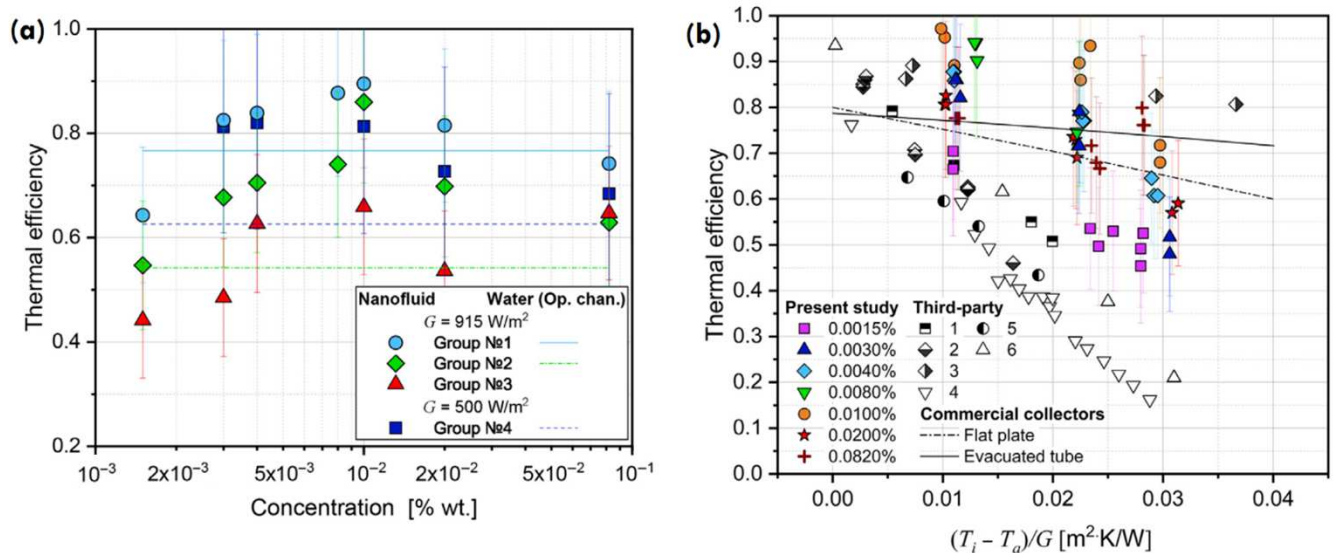
Figure 9. Thermal efficiency of a DASC operating with different nanofluids. (**a**) Thermal efficiency vs. nanoparticle concentration. (**b**) Comparison based on thermal efficiency. Modified and printed with permission from [78].

Wang et al. [80] modified the typical DASC model with the addition of a separation tank. In the modified experimental setup, the rotating magnetic field as an external forced convective system was added to achieve non-uniform solar irradiation. This modification results in an increase in photothermal efficiency by up to 12.8% due to the change in the heating mechanism from conduction to convection. The main reason for this is that the

heat transfer mechanism of working fluids is changed from heat conduction to thermal convection, which decreases heat loss to the environment. Moreover, the method is effective to reduce the flow losses and blockage in the pipeline. The modified DASC model is shown in Figure 10.

Figure 10. Experimental DASC setup. (**a**) DASC without magnetic separation tank. (**b**) DASC with magnetic separation tank [80].
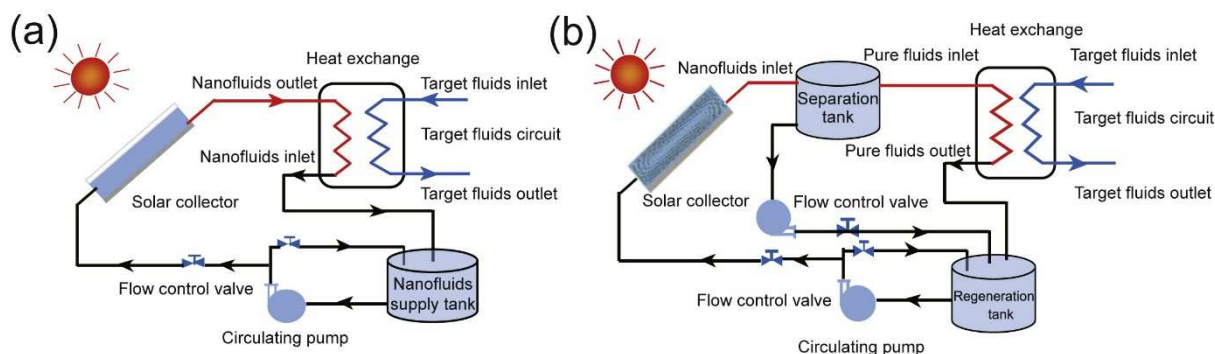
Hooshmand et al. [81] developed the porous-foam-filled DASC system. The 12 mm air gap was created between the double-pane collector glazing, and polyurethane foam was filled to reduce the heat losses. The enhancement in thermal efficiency was observed by utilizing both porous foam and SiC nanoparticles in the working fluid. Zhang et al. [82] developed a novel DASC by utilizing the TiN/GO hybrid nanofluid and heat storage core made of molten salt (44% KNO_3, 12% $NaNO_3$, and 44% $Ca(NO_3)_2$,). The maximum experimental collector efficiency was 526.96 J. Based on the concept of the cavity, Peng et al. [83] developed the novel DASC model, in which a cavity-type receiver tube was equipped with parabolic reflectors. The modified novel DASC is shown in Figure 11. In this DASC, two parabolic concave mirrors were installed to focus the solar rays and transfer them to the receiver. The schematic of the novel DASC and cross-section of the tube is shown in Figure 11a. The effect of different reflection shapes on efficiency was noticed. Figure 11b shows the comparison of the efficiency of a novel collector with a conventional DASC and a surface-based solar collector (SBSC).

Qin et al. [84] designed a direct-absorption parabolic-trough solar collector (DAPTSC) to achieve the effect of both surface and volumetric absorption. The two nanofluids were used separately in two sections of a DAPTSC. Low concentrated nanofluid was used in the outer segment, while the high concentrated nanofluid was used in the inner section. The semi-cylindrical coating was used for making the DAPTSC capable of both surface and direct absorption. A significant enhancement in thermal efficiency was observed using a hybrid DAPTSC. Kumar et al. [85] suggested three different designs of DASC based on the shape of the absorber plates, such as trapezoidal-corrugated DASC, triangular-corrugated DASC, and circular-corrugated DASC. The heat transfer area was varied by changing the shape of the absorber plate. All of the configurations are shown in Figure 12. Maximum thermal efficiency was obtained for circulated–corrugated DASC.

Karami et al. [86] developed the DASC system combined with a humidification-dehumidification desalination unit. The proposed system reduces significant heat losses. Many other design parameters, such as receiver thickness, tube shape, etc., have been also considered by a few authors. The literature indicates that design modification is the most important parameter for nanofluid-based DASCs.
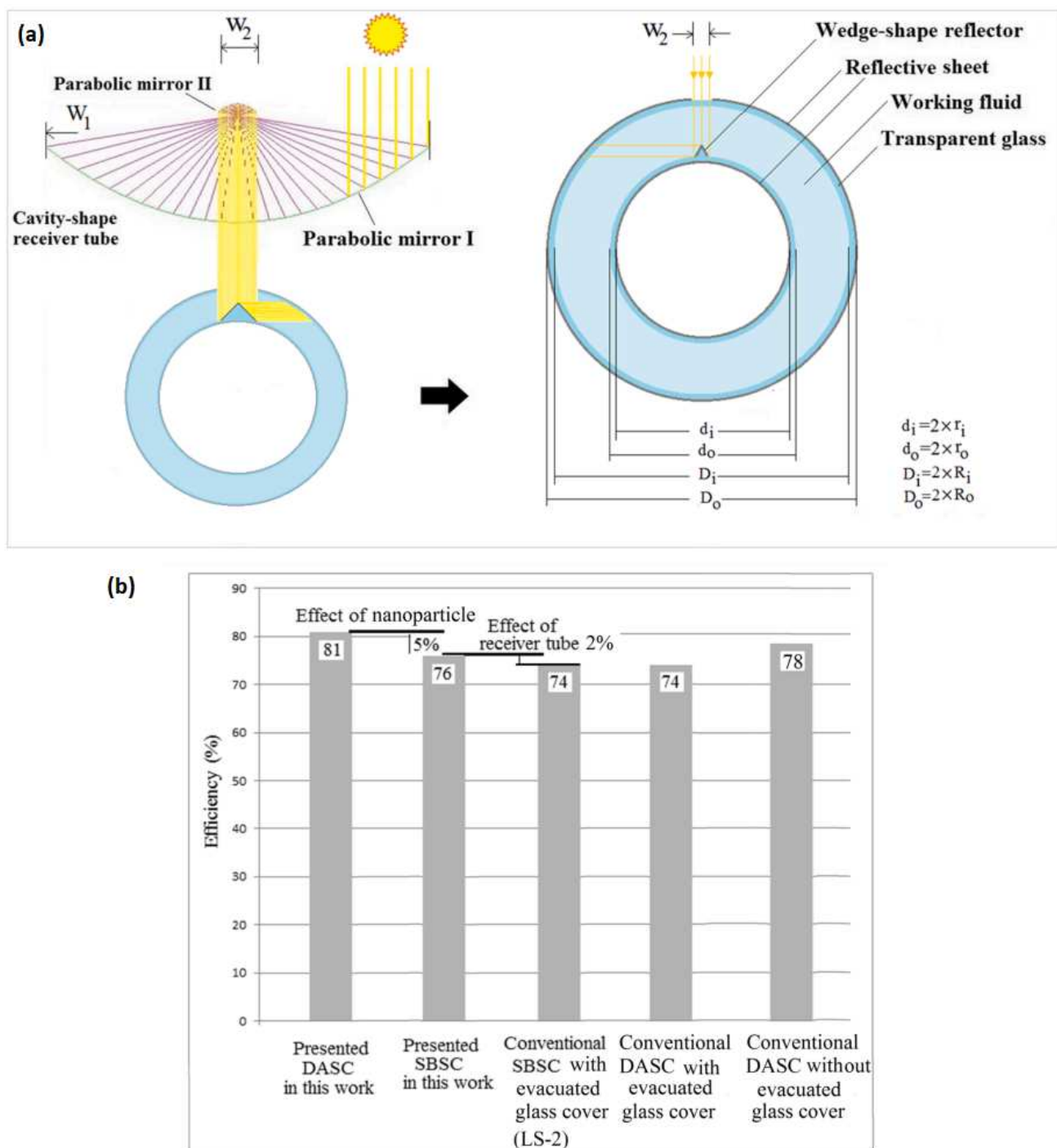
Figure 11. (**a**) Schematic of a newly designed DASC and the cross-section of receiver tube. (**b**) Comparison of developed DASC and SBSC models with conventional models. Modified and printed with permission from [83].
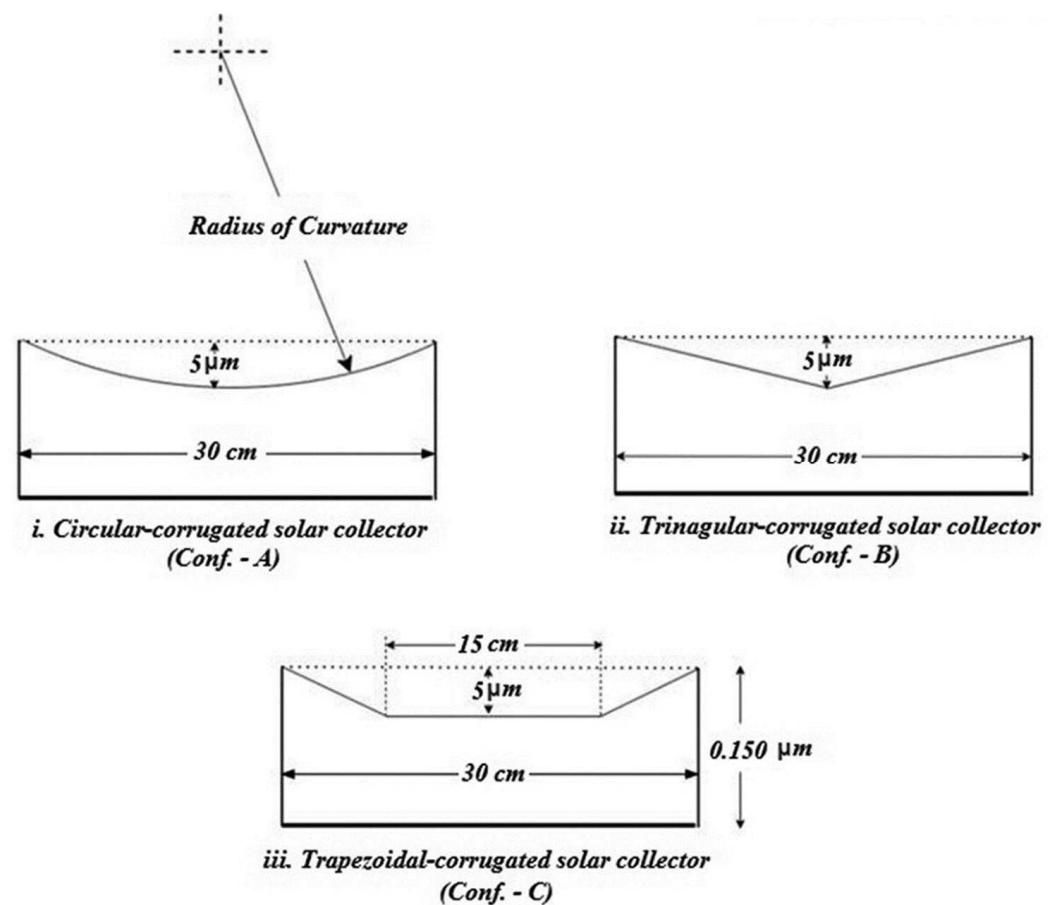
Figure 12. Configurations of absorber plates. Modified and printed with permission from [85].

4. Operating Parameters

4.1. Temperature

At elevated temperatures, thermal conductivity rises because of energized nanoparticles. Frictional resistance between adjoining layers and enhanced Brownian motion is the cause of this enhanced thermal conductivity, whereas working fluid viscosity decreases with a temperature rise.

4.2. Flow Rate

The flow rate strongly affects the performance of the DASC. The results of many studies showed that the collector efficiency increases with the increasing flow rate of working fluids [87], whereas the exergy efficiency decreases [88]. The outlet temperature decreases with increasing flow rate due to the decrease in solar radiation absorption. Thakur et al. [89] studied the effect of flow rate on pumping power, entropy growth rate, and exergy efficiency using a DASC. The results of the study are presented in Figure 13. Vakili et al. [35] studied the influence of flow rate on DASC collector performance. It was found that a 0.00075 kg/s flow rate gave the worst collector performance, and the performance of the collector was improved at a flow rate of 0.015 kg/s.
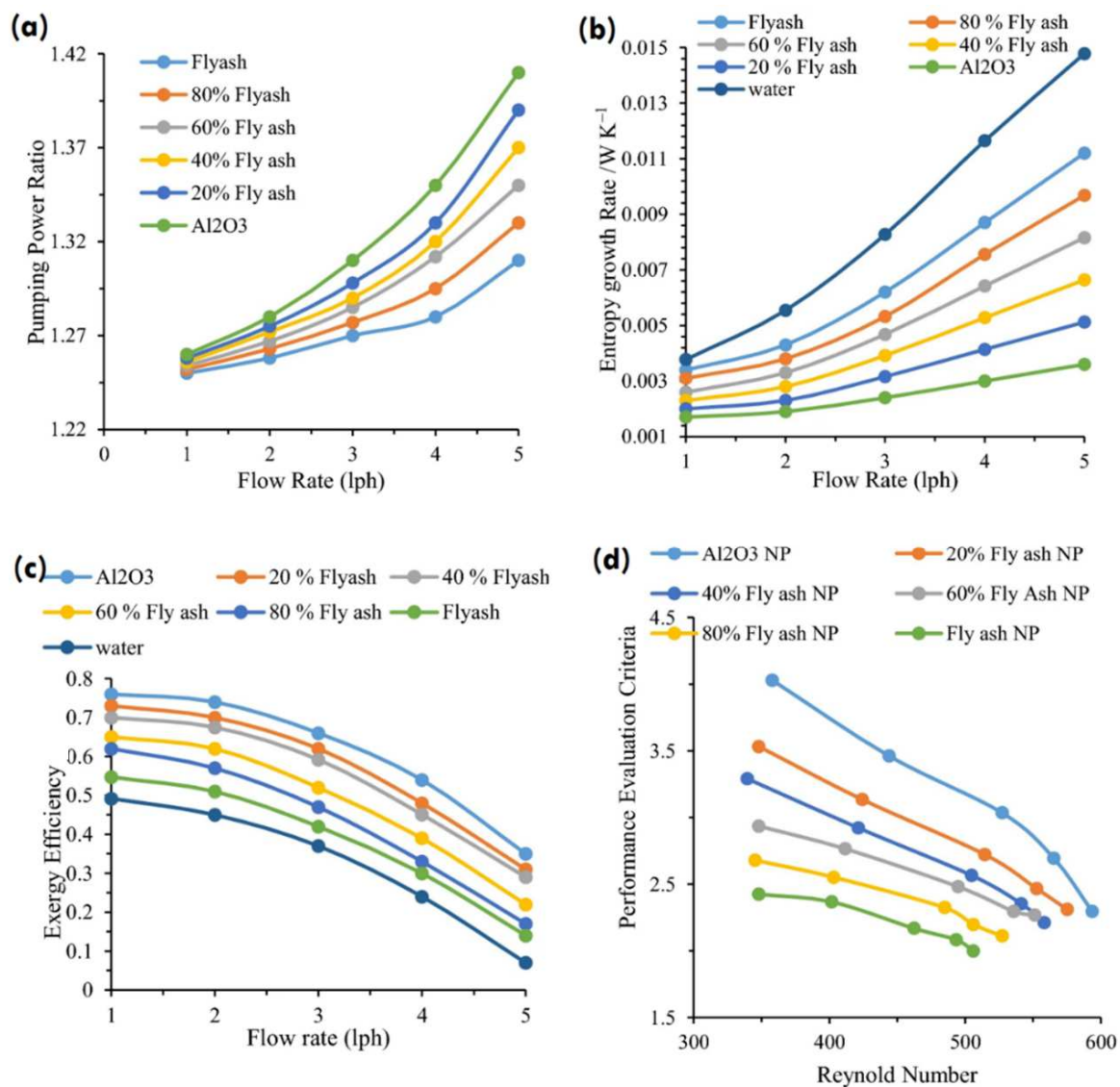
Figure 13. Effect of flow rate on the performance of DASC operating with different nanofluids. (**a**) Pumping power vs. flow rate (**b**) Entropy growth rate vs. flow rate. (**c**) Exergy efficiency vs. flow rate. (**d**) Performance evaluation criteria vs. Reynold number. Modified and printed with permission from [89].

4.3. Flow Regime

The heat transfer performance of a DASC increases with the change in flow regime from laminar to turbulent. The convective coefficient of the DASC is increased by increasing the Reynolds number and increasing the Nusselt number [90]. The collector efficiency is enhanced up to a certain limit of Reynolds number, and then decreases at a higher Reynolds number due to the higher heat loss. Moreover, the entropy generation and pressure drop at higher Reynolds numbers become higher due to more friction as the result of inertial forces. Some studies [91] showed that the heat transfer properties change in different light regions.

4.4. Penetration Depth

The coolant in the DASC must have low transmissivity and high absorptivity over a different range of wavelengths. Hazara et al. [92] studied the optical characteristics of nanofluids in DASCs, and studied the effect of nanoparticle size and concentration on a wide range of wavelengths. The results of the study are presented in Figure 14. The increase in scattering and reduction in transmittance was observed by the increasing

nanoparticle concentration and size. The reduction of transmittance is due to the increased light scattering by the nanoparticles present in the fluid. This leads to decreased absorption capability.
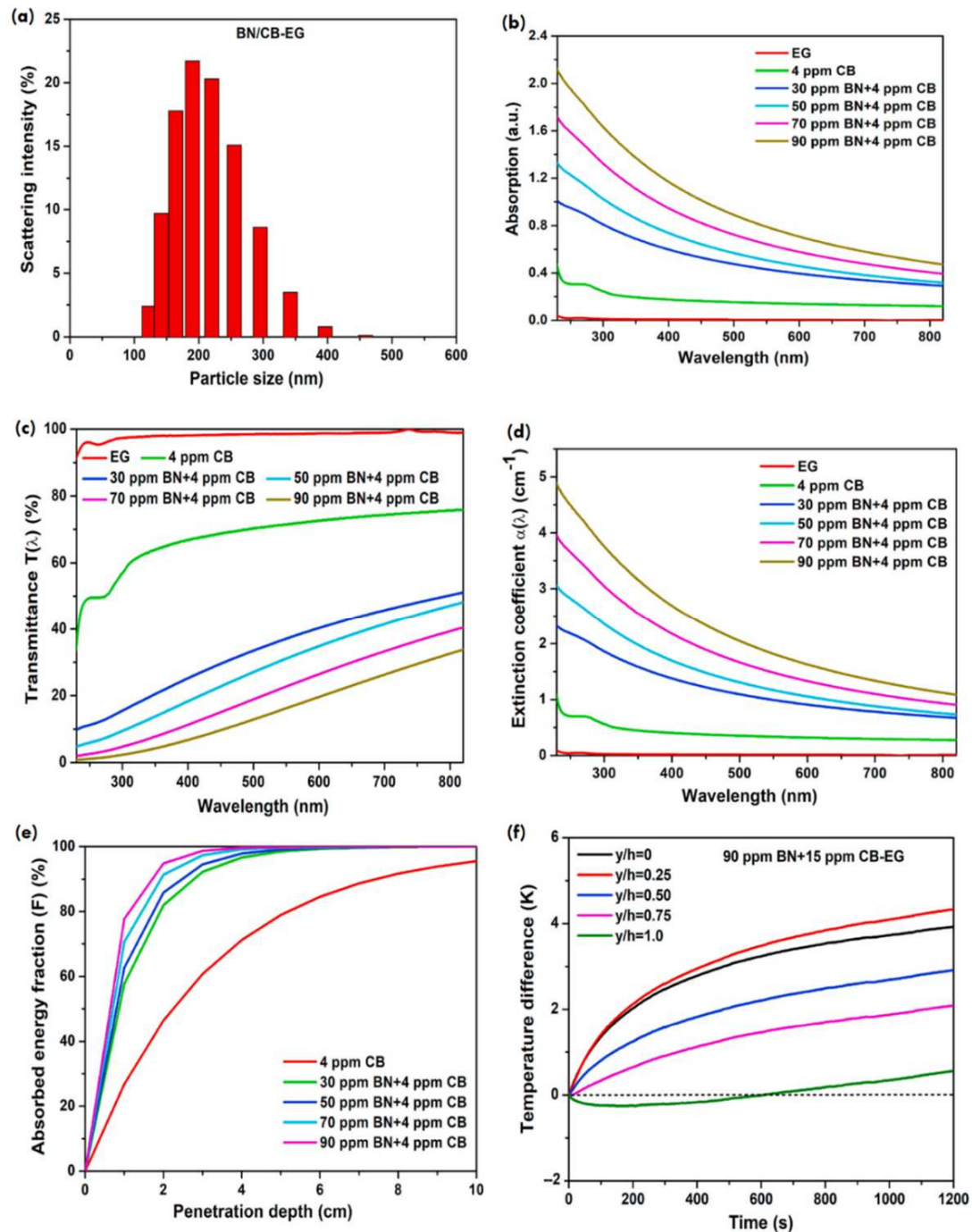
Figure 14. Optical characteristics of boron nitride (BN)/carbon black ethylene glycol nanofluids. (**a**) Scattering intensity at various particle sizes. (**b**) Absorption spectra at various wavelengths; transmittance spectra at various wavelengths. (**c**) Transmittance spectra at various wavelengths. (**d**) Extinction coefficients at various wavelengths. (**e**) Absorbed energy fraction at various penetration depths (fluid height from the top level to inside the collector). (**f**) Temperature difference vs. exposure time at various fluid heights. Modified and printed with permission from [92].

An increase in the size of nanoparticles and their concentration results in an increased scattering, which in turn decreases the optical absorption capability. The performance of a DASC is excessively influenced by the effect of absorption and scattering. This scattering and optical absorption behavior influence the extinction coefficient of a working fluid.

4.5. Irradiation Position

Wang et al. [93] studied the effect of solar irradiation position by developing the two test configurations of DASC systems, such as bottom irradiation DASC and side irradiation DASC. The results show that the bottom irradiation DASC collector exhibited better performance as compared to the side irradiation DASC system. The results of the study for both configurations are presented in Figure 15.
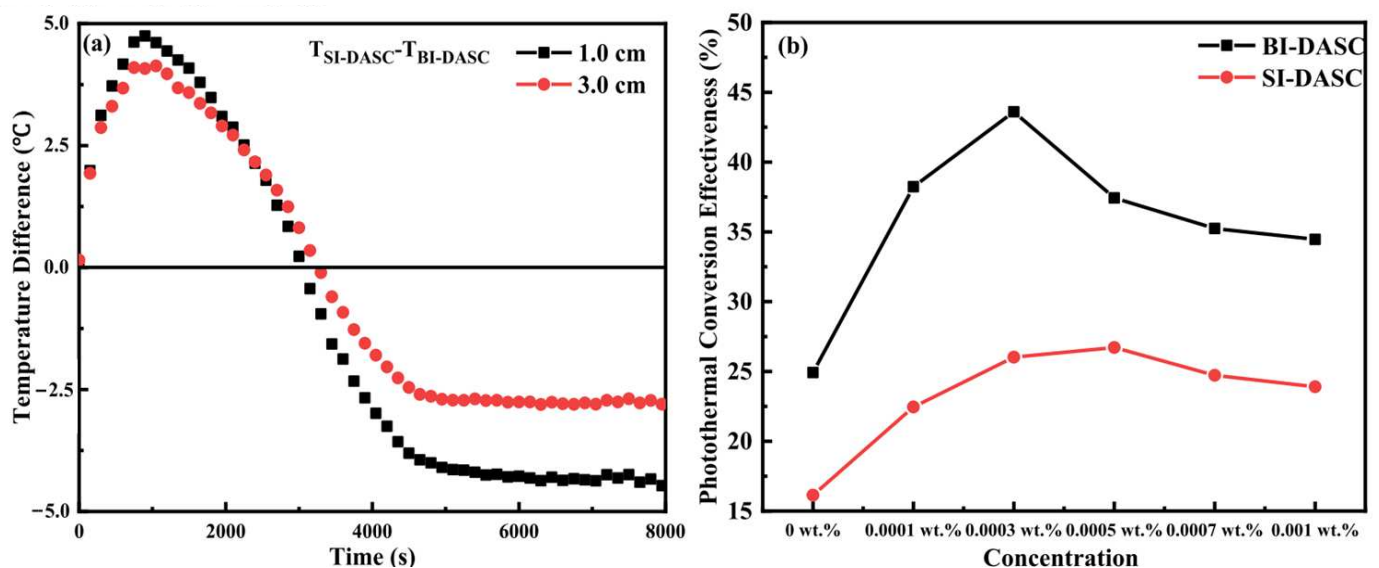

Figure 15. Effect of irradiation position on DASC configuration. (**a**) Temperature difference at different depths. (**b**) Photothermal conversion effectiveness for bottom irradiation (BI) and side irradiation (SI) DASC systems. Modified and printed with permission from [93].

Shen et al. [94] developed a model for investigating the effect of effective radius, length-radius ratio, and incident light angle of nanoparticles on the performance of DASC. The optimum value of each parameter was investigated. The simulation results showed that the nanoparticle's effective radius has a significant influence on the transmittance. It is evident from the results that the effective radius also has a significant effect on the directional-hemispherical transmittance. The figure shows the hemispherical transmittances of rod-shaped Au nanofluids with different length-radius (L/R) ratios, such as 6, 7, and 8. For each L/R ratio, the two peaks of transmittance are shown. The transmittances of Au nanofluids at different angles of incidence are shown in Figure 16. When electromagnetic waves propagate radially concerning the Au nanorods, the transmissivity decreases. Transmittance reduces in the same spectral region in which the electromagnetic wave is incident radially to the particles. Figure 16d shows the solar absorption spectrum of Au nanofluids, with different incident angles.
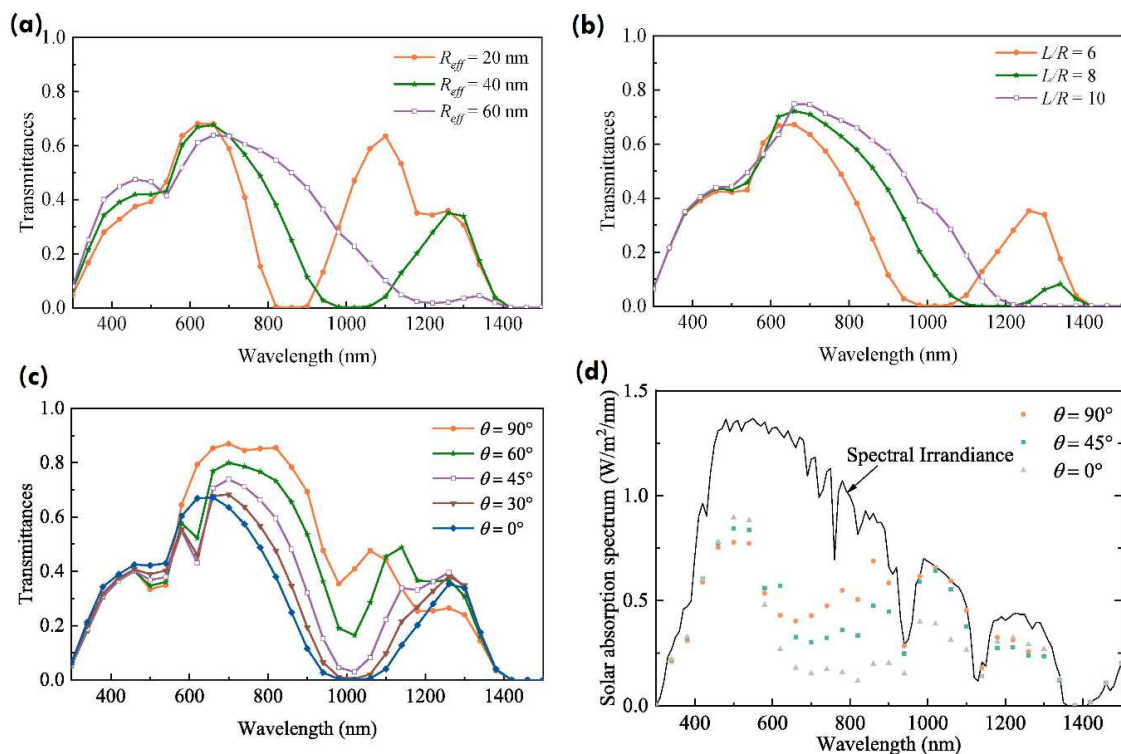
Figure 16. Effect of different radius sizes, length/radius, and angle of incidence on transmittance and solar absorption. (**a**) Effect of radius size on transmittance. (**b**) Effect of different length/radius on transmittance. (**c**) Effect of incidence angle on transmittance. (**d**) Effect of incidence angle on solar absorption. Modified and printed with permission from [94].

Zhu et al. [95] studied the radiative effects, including absorption, emission, and scattering, on DASCs. The results showed that DASCs have both benefits and disadvantages over SBSCs. Sharaf at al. [96] investigated the influence of the type of radiation spectrum under different operating conditions for several working fluids in DASCs. Many other operating parameters, such as inlet flow velocity, radiative heat flux, and aspect ratio, are considered. The results of many other studies are reported in Table 1. Most of the effective parameters and their values are reported. The reported results show that the performance of a DASC can be enhanced by optimizing the working fluid parameters, collector dimensions, flow rate, and solar irradiance.

Table 1. Summary of Results.

Ref.	Solar System	Working Fluid Properties	Operating Parameters	Collector Design Parameters	Results
[97]	DASC	Base fluid—Water Nanoparticle Type—CuO/ZnO Particle size—30/50 nm Particle concentration—0.01 vol% (70:30)	Irradiance—1000 W/m^2	Panel Type—Quartz cuvette Size—2.5 × 12.5 × 45 mm	Thermal conductivity—+10% Transmittance—−100% Rise in temperature—15% Extinction coefficient—+100% Photo Thermal efficiency—97.35%
[98]	DASC	Base fluid—DI water Nanoparticle Type—Al$_2$O$_3$/Co$_3$O$_4$ Sample Thickness—10–30 mm Mass fraction—40 mg/L	Incident flux—8.5 W/cm^2	Diameter—20 mm Height—30 mm	Solar Absorptivity—+80% Penetration depth—20 mm Temperature rise—+5.4%

Table 1. *Cont.*

Ref.	Solar System	Working Fluid Properties	Operating Parameters	Collector Design Parameters	Results
[99]	DASC	Base fluid—DI water Nanoparticle Type—Ag/rGO Ag particle size—25 to 45 nm Particle concentration—40 ppm	Irradiance—1326 W/m^2	Inner diameter—30 mm Collector Height—20 mm	Enhancement in collector efficiency—2.7 Times Collector efficiency—+77% Transmittance—−21% Extinction coefficient—+20%
[16]	DASC	Base fluid—water Nanoparticle type—SiO$_2$/Au Particle size—10 nm core radius & 10 nm shell thickness Particle concentration—0.01 vol%	Mass flow rate—0.004 kg/ms	Collector length—1 m Collector height—1.5 cm Height variation—1–2 cm	Collector Efficiency—25%
[100]	DASC	Base fluid—water Nanoparticle type—CuO/MWCNT Particle size Ag—25–45 nm Particle concentration—0.0015 wt.%	—	Inner diameter—30 mm Outer diameter—45 mm Length—200 mm	Rise in temperature—+13.3% Transmittance—−530% Solar weighted absorption fraction—+233% Extinction coefficient—+500%
[101]	DASC	Base fluid—water Nanoparticle type—Fe$_3$O$_4$/SiO$_2$ Particle size—400–500 nm Mass fraction—1 mg/mL	Irradiance—1000 W/m^2	Tube diameter—3.6 cm Collector height—5 cm	Temperature rise—+108% Enhancement in photothermal conversion efficiency—32.9% Efficiency—98.5%
[102]	DASC	Base fluid—DI Water Nanoparticle type—Au/Cu Particle size—2 to 3 nm Particle concentration—150/2000 mg/L	Irradiance—1000 W/m^2	—	Temperature Rise—+60–100%
[14]	DASC	Base fluid—DI Water Nanoparticle type—Au/Ag Particle size—29 ± 7 nm Volume fraction—0.00025%	—	—	Photothermal conversion efficiency—+41.37%
[103]	DASC	Base fluid—DI Water Nanoparticle type—Fe$_3$SO$_4$/SiO$_2$ Particle size—30/15 nm Volume fraction—500 ppm, 1000 ppm & 2000 ppm Volume ratio—25:75, 50:50 & 75:25	—	Collector size—60 × 60 × 1 cm	Exergy efficiency—+63.7% Collector efficiency—+16.6% Extinction coefficient—+800%
[104]	DASC	Base fluid—Silicone oil Nanoparticle type—ZnO/Au Particle size—80/13.3 nm Particle concentration—0.1, 0.5 & 1.0 mg/mL	Irradiance—10 k W/m^2	—	Photothermal Efficiency—+240%
[87]	DASC	Base fluid—DI water Nanoparticle type—Al$_2$O$_3$ Particle size—5 nm Mass fraction—20 to 100 mg/L	Irradiance—1000 W/m^2 Mass flow rate—0.010 kg/s	Collector length—1 m Collector width—1 m Height of collector—6 to 12 m	Collector efficiency—38–85% Outlet temperature—28 to 80 °C

Table 1. *Cont.*

Ref.	Solar System	Working Fluid Properties	Operating Parameters	Collector Design Parameters	Results
[105]	DASC	Base fluid—water Nanoparticle Type—Al, Au, Cu & Graphite	Irradiance—1000 W/m^2	Length—5 cm Width—3 cm Height—150 μm	—
[106]	DASC	Base fluid—DI water Nanoparticle Type—PVP (polyvinylpyrrolidone) coated silver Density 10.5 g/cm^3 Volume fraction—250 ppm, 500 ppm & 1000 ppm	Tilt angle—20°, 35°, 50° Flow rate—0.0075 kg/s, 0.015 kg/s & 0.0225 kg/s	60 × 60 × 1 cm	—
[18]	DASC	Base fluid—water Nanoparticle Type—Graphite Particle size–30 nm	1000 W/m^2	Collector size—3 × 5 cm^2 Collector depth—150 μm	Efficiency—84% Exergy efficiencies—94.3%

5. Conclusions and Future Challenges

Solar energy is a plausible solution to the world's energy crisis issue due to its low installation and maintenance cost, huge potential, and feasibility of installation. Due to its performance, the DASC has outperformed the other collectors. The effectiveness of the DASC is dependent on various aspects. This review summarizes the effect of design and working parameters on the performance of DASCs. The following points have been concluded from this review.

Ethylene glycol has superior thermal properties in DASCs as compared to water, and engine oil also has superior thermal properties in comparison to water. Additionally, the mixture of ethylene glycol and water can be used to enhance thermal properties.

The performance of the DASC operated with carbon-based nanofluids was found to be higher as compared to the DASC operated with any other working fluid, under the same operating conditions. The addition of carbon nanoparticles in working fluid is useful for enhancing the solar absorption capability and thermal performance of DASCs.

A smaller nanoparticle size is beneficial in DASCs for improving the optical characteristics of nanofluids. Smaller-sized nanoparticles exhibit less transmittance and absorb light in a better way.

The nanofluids made of sharp-edged or cubic particles exhibit higher absorption properties and thermal conductivity as compared to spherical or rod-shaped nanoparticles. The platelet-shaped or cylindrical particles induce higher performance in terms of entropy, viscosity generation, and thermal conductivity. Moreover, the nanoparticles with anisotropic characteristics and multiple surfaces show higher absorption and thermal properties.

The maximum efficiency of a DASC can be achieved up to a certain limit of particle concentration; beyond this, the efficiency is decreased. At higher volume fractions, the viscosity is increased due to the increase in non-Newtonian behavior, which results in increasing the pumping power.

An increase in the length of the solar panel results in an increased surface area, which helps solar panels to capture more solar radiation. However, it was observed that after a certain limit, the performance of the solar panel deteriorates, which results in additional heat loss. The exergy effectiveness enhances with an increase in collector length up to an extent, after which it begins reducing. In order to gain the most useful power, an appropriate fluid velocity according to the collector length must be selected.

The thermal efficiency of a DASC is highly dependent on the collector thickness. The maximum performance can be achieved by investigating the optimum thickness of the receiver.

Many novel DASC designs, such as the tabular DASC, the DASC with a rotating magnetic field as an external forced convective system, the porous-foam filled DASC, the direct-absorption parabolic-trough solar collector (DAPTSC), and circulated–corrugated DASC can be used to enhance the performance of DASCs as compared to conventional DASCs. At elevated temperatures, thermal conductivity rises because of energized nanoparticles. Frictional resistance between adjoining layers and enhanced Brownian motion is the cause of this enhanced thermal conductivity, whereas working fluid viscosity decreases with a rise in temperature. The collector efficiency increases with the increasing flow rate of the working fluid, whereas the exergy efficiency decreases. The outlet temperature decreases with increasing flow rate due to the decrease in solar radiation absorption.

The heat transfer performance of a DASC increases with the change in a flow regime from laminar to turbulent. The convective coefficient of the DASC increases by increasing the Reynolds number and increasing the Nusselt number. The collector efficiency is enhanced up to a certain limit of the Reynolds number, and then decreases at a higher Reynolds number due to the higher heat loss. Moreover, the entropy generation and pressure drop at higher Reynolds numbers become higher due to more friction as the result of inertial forces.

The effect of the solar irradiation position is also important. The bottom irradiation DASC collector exhibits better performance as compared to the side irradiation DASC system. The DASC has both benefits and disadvantages over surface absorption collectors.

Most of the effective parameters reported in the different sections are dependent on each other. Most of these authors studied the influence of only a few parameters on the performance of DASC by considering the constant values of other parameters. So, the constraints of each reported study limited this study. As the concluding remarks are reported based on the reported literature, the parameter values cannot be used directly to optimize the performance of DASCs. Hence, there is a need to consider all effective parameters and their influence on DASC efficiency under the same operating conditions.

Author Contributions: Writing—original draft, investigation, M.H.; methodology, formal analysis, S.K.H.S.; formal analysis, review and editing, U.S.; review and editing, supervision, funding acquisition, N.A.; methodology, formal analysis, A.A. All authors have read and agreed to the published version of the manuscript.

Data Availability Statement: Not applicable.

Conflicts of Interest: The authors declare no conflict of interest.

References

1. Shah, T.R.; Babar, H.; Ali, H.M. Energy Harvesting: Role of Hybrid Nanofluids. In *Emerging Nanotechnologies for Renewable Energy*; Elsevier: Amsterdam, The Netherlands, 2021; pp. 173–211. ISBN 9780128212059.
2. Sharaf, O.Z.; Taylor, R.A.; Abu-Nada, E. On the Colloidal and Chemical Stability of Solar Nanofluids: From Nanoscale Interactions to Recent Advances. *Phys. Rep.* **2020**, *867*, 1–84. [CrossRef]
3. Sharaf, O.Z.; Rizk, N.; Munro, C.J.; Joshi, C.P.; Anjum, D.H.; Abu-Nada, E.; Martin, M.N.; Alazzam, A. Radiation Stability and Photothermal Performance of Surface-Functionalized Plasmonic Nanofluids for Direct-Absorption Solar Applications. *Sol. Energy Mater. Sol. Cells* **2021**, *227*, 111115. [CrossRef]
4. Sharaf, O.Z.; Rizk, N.; Munro, C.J.; Joshi, C.P.; Waheed, W.; Abu-Nada, E.; Alazzam, A.; Martin, M.N. Thermal Stability and Plasmonic Photothermal Conversion of Surface-Modified Solar Nanofluids: Comparing Prolonged and Cyclic Thermal Treatments. *Energy Convers. Manag.* **2021**, *244*, 114463. [CrossRef]
5. Sharaf, O.Z.; Rizk, N.; Joshi, C.P.; Abi Jaoudé, M.; Al-Khateeb, A.N.; Kyritsis, D.C.; Abu-Nada, E.; Martin, M.N. Ultrastable Plasmonic Nanofluids in Optimized Direct Absorption Solar Collectors. *Energy Convers. Manag.* **2019**, *199*, 112010. [CrossRef]
6. Mahesh, A. Solar Collectors and Adsorption Materials Aspects of Cooling System. *Renew. Sustain. Energy Rev.* **2017**, *73*, 1300–1312. [CrossRef]
7. Yan, S.; Wang, F.; Shi, Z.G.; Tian, R. Heat Transfer Property of SiO_2/Water Nanofluid Flow inside Solar Collector Vacuum Tubes. *Appl. Therm. Eng.* **2017**, *118*, 385–391. [CrossRef]
8. Li, S.; Wang, H.; Meng, X.; Wei, X. Comparative Study on the Performance of a New Solar Air Collector with Different Surface Shapes. *Appl. Therm. Eng.* **2017**, *114*, 639–644. [CrossRef]

9. Touaba, O.; Ait Cheikh, M.S.; Slimani, M.E.A.; Bouraiou, A.; Ziane, A.; Necaibia, A.; Harmim, A. Experimental Investigation of Solar Water Heater Equipped with a Solar Collector Using Waste Oil as Absorber and Working Fluid. *Sol. Energy* **2020**, *199*, 630–644. [CrossRef]

10. Ahmadlouydarab, M.; Ebadolahzadeh, M.; Muhammad Ali, H. Effects of Utilizing Nanofluid as Working Fluid in a Lab-Scale Designed FPSC to Improve Thermal Absorption and Efficiency. *Phys. A Stat. Mech. Its Appl.* **2020**, *540*, 123109. [CrossRef]

11. Goel, N.; Taylor, R.A.; Otanicar, T. A Review of Nanofluid-Based Direct Absorption Solar Collectors: Design Considerations and Experiments with Hybrid PV/Thermal and Direct Steam Generation Collectors. *Renew. Energy* **2020**, *145*, 903–913. [CrossRef]

12. Deng, Z.; Zhou, J.; Miao, L.; Liu, C.; Peng, Y.; Sun, L.; Tanemura, S. The Emergence of Solar Thermal Utilization: Solar-Driven Steam Generation. *J. Mater. Chem. A* **2017**, *5*, 7691–7709. [CrossRef]

13. Bårdsgård, R.; Kuzmenkov, D.M.; Kosinski, P.; Balakin, B.V. Eulerian CFD Model of Direct Absorption Solar Collector with Nanofluid. *J. Renew. Sustain. Energy* **2020**, *12*, 033701. [CrossRef]

14. Chen, M.; He, Y.; Zhu, J. Preparation of Au–Ag Bimetallic Nanoparticles for Enhanced Solar Photothermal Conversion. *Int. J. Heat Mass Transf.* **2017**, *114*, 1098–1104. [CrossRef]

15. Esmaeili, M.; Karami, M.; Delfani, S. Performance Enhancement of a Direct Absorption Solar Collector Using Copper Oxide Porous Foam and Nanofluid. *Int. J. Energy Res.* **2020**, *44*, 5527–5544. [CrossRef]

16. Won, K.H.; Lee, B.J. Effect of Light Scattering on the Performance of a Direct Absorption Solar Collector. *Front. Energy* **2018**, *12*, 169–177. [CrossRef]

17. Zeiny, A.; Jin, H.; Lin, G.; Song, P.; Wen, D. Solar Evaporation via Nanofluids: A Comparative Study. *Renew. Energy* **2018**, *122*, 443–454. [CrossRef]

18. Gorji, T.B.; Ranjbar, A.A. Thermal and Exergy Optimization of a Nanofluid-Based Direct Absorption Solar Collector. *Renew. Energy* **2017**, *106*, 274–287. [CrossRef]

19. Chen, W.; Zou, C.; Li, X. An Investigation into the Thermophysical and Optical Properties of SiC/Ionic Liquid Nanofluid for Direct Absorption Solar Collector. *Sol. Energy Mater. Sol. Cells* **2017**, *163*, 157–163. [CrossRef]

20. Chamsa-ard, W.; Brundavanam, S.; Fung, C.; Fawcett, D.; Poinern, G. Nanofluid Types, Their Synthesis, Properties and Incorporation in Direct Solar Thermal Collectors: A Review. *Nanomaterials* **2017**, *7*, 131. [CrossRef]

21. Qin, C.; Kang, K.; Lee, I.; Lee, B.J. Optimization of the Spectral Absorption Coefficient of a Plasmonic Nanofluid for a Direct Absorption Solar Collector. *Sol. Energy* **2018**, *169*, 231–236. [CrossRef]

22. Mallah, A.R.; Mohd Zubir, M.N.; Alawi, O.A.; Salim Newaz, K.M.; Mohamad Badry, A.B. Plasmonic Nanofluids for High Photothermal Conversion Efficiency in Direct Absorption Solar Collectors: Fundamentals and Applications. *Sol. Energy Mater. Sol. Cells* **2019**, *201*, 110084. [CrossRef]

23. Campos, C.; Vasco, D.; Angulo, C.; Burdiles, P.A.; Cardemil, J.; Palza, H. About the Relevance of Particle Shape and Graphene Oxide on the Behavior of Direct Absorption Solar Collectors Using Metal Based Nanofluids under Different Radiation Intensities. *Energy Convers. Manag.* **2019**, *181*, 247–257. [CrossRef]

24. Sarafraz, M.M.; Tian, Z.; Tlili, I.; Kazi, S.; Goodarzi, M. Thermal Evaluation of a Heat Pipe Working with N-Pentane-Acetone and n-Pentane-Methanol Binary Mixtures. *J. Therm. Anal. Calorim. 2019 1394* **2019**, *139*, 2435–2445. [CrossRef]

25. Abdelrazik, A.S.; Tan, K.H.; Aslfattahi, N.; Arifutzzaman, A.; Saidur, R.; Al-Sulaiman, F.A. Optical, Stability and Energy Performance of Water-Based MXene Nanofluids in Hybrid PV/Thermal Solar Systems. *Sol. Energy* **2020**, *204*, 32–47. [CrossRef]

26. Babar, H.; Ali, H.M. Towards Hybrid Nanofluids: Preparation, Thermophysical Properties, Applications, and Challenges. *J. Mol. Liq.* **2019**, *281*, 598–633. [CrossRef]

27. Menni, Y.; Chamkha, A.J.; Massarotti, N.; Ameur, H.; Kaid, N.; Bensafi, M. Hydrodynamic and Thermal Analysis of Water, Ethylene Glycol and Water-Ethylene Glycol as Base Fluids Dispersed by Aluminum Oxide Nano-Sized Solid Particles. *Int. J. Numer. Methods Heat Fluid Flow* **2020**, *30*, 4349–4386. [CrossRef]

28. Gholinia, M.; Hosseinzadeh, K.; Ganji, D.D. Investigation of Different Base Fluids Suspend by CNTs Hybrid Nanoparticle over a Vertical Circular Cylinder with Sinusoidal Radius. *Case Stud. Therm. Eng.* **2020**, *21*, 100666. [CrossRef]

29. Gao, Y.; Wang, H.; Sasmito, A.P.; Mujumdar, A.S. Measurement and Modeling of Thermal Conductivity of Graphene Nanoplatelet Water and Ethylene Glycol Base Nanofluids. *Int. J. Heat Mass Transf.* **2018**, *123*, 97–109. [CrossRef]

30. Cao, P.; Li, Y.; Wu, Y.; Chen, H.; Zhang, J.; Cheng, L.; Niu, T. Role of Base Fluid on Enhancement Absorption Properties of Fe_3O_4/Ionic Liquid Nanofluids for Direct Absorption Solar Collector. *Sol. Energy* **2019**, *194*, 923–931. [CrossRef]

31. Abbas, N.; Awan, M.B.; Amer, M.; Ammar, S.M.; Sajjad, U.; Ali, H.M.; Zahra, N.; Hussain, M.; Badshah, M.A.; Jafry, A.T. *Applications of Nanofluids in Photovoltaic Thermal Systems: A Review of Recent Advances*; Elsevier B.V.: Amsterdam, The Netherlands, 2019; Volume 536, p. 122513.

32. Ahmad, H.; Al-Khaled, K.; Sowayan, A.S.; Abdullah, M.; Hussain, M.; Hammad, A.; Khan, S.U.; Tlili, I. Experimental Investigation for Automotive Radiator Heat Transfer Performance with $ZnO–Al_2O_3$/Water-Based Hybrid Nanoparticles: An Improved Thermal Model. *Int. J. Mod. Phys. B* **2022**, *36*, 2350050. [CrossRef]

33. Hu, G.; Ning, X.; Hussain, M.; Sajjad, U.; Sultan, M.; Ali, H.M.; Shah, T.R.; Ahmad, H. Potential Evaluation of Hybrid Nanofluids for Solar Thermal Energy Harvesting: A Review of Recent Advances. *Sustain. Energy Technol. Assess.* **2021**, *48*, 101651. [CrossRef]

34. Wang, H.; Li, X.; Luo, B.; Wei, K.; Zeng, G. The MXene/Water Nanofluids with High Stability and Photo-Thermal Conversion for Direct Absorption Solar Collectors: A Comparative Study. *Energy* **2021**, *227*, 120483. [CrossRef]

35. Vakili, M.; Yahyaei, M.; Ramsay, J.; Aghajannezhad, P.; Paknezhad, B. Adaptive Neuro-Fuzzy Inference System Modeling to Predict the Performance of Graphene Nanoplatelets Nanofluid-Based Direct Absorption Solar Collector Based on Experimental Study. *Renew. Energy* **2021**, *163*, 807–824. [CrossRef]

36. Zheng, N.; Yan, F.; Wang, L.; Sun, Z. Photo-Thermal Conversion Performance of Mono MWCNT and Hybrid MWCNT-TiN Nanofluids in Direct Absorption Solar Collectors. *Int. J. Energy Res.* **2022**, *46*, 8313–8327. [CrossRef]

37. Joseph, A.; Thomas, S. Energy, Exergy and Corrosion Analysis of Direct Absorption Solar Collector Employed with Ultra-High Stable Carbon Quantum Dot Nanofluid. *Renew. Energy* **2022**, *181*, 725–737. [CrossRef]

38. Kumar, P.G.; Vigneswaran, S.; Meikandan, M.; Sakthivadivel, D.; Salman, M.; Thakur, A.K.; Sathyamurthy, R.; Kim, S.C. Exploring the Photo-Thermal Conversion Behavior and Extinction Coefficient of Activated Carbon Nanofluids for Direct Absorption Solar Collector Applications. *Environ. Sci. Pollut. Res.* **2022**, *29*, 13188–13200. [CrossRef]

39. Hazra, S.K.; Ghosh, S.; Nandi, T.K. Photo-Thermal Conversion Characteristics of Carbon Black-Ethylene Glycol Nanofluids for Applications in Direct Absorption Solar Collectors. *Appl. Therm. Eng.* **2019**, *163*, 114402. [CrossRef]

40. Warjri, M.; Narayan, J. Synthesis, Characterization and Physicochemical Properties of Cupric Oxide Nanoparticles and Their Nanofluids. In Proceedings of the Materials Today: Proceedings; Elsevier Ltd.: Amsterdam, The Netherlands, 2019; Volume 18, pp. 1176–1184.

41. Suganthi, K.S.; Rajan, K.S. Metal Oxide Nanofluids: Review of Formulation, Thermo-Physical Properties, Mechanisms, and Heat Transfer Performance. *Renew. Sustain. Energy Rev.* **2017**, *76*, 226–255. [CrossRef]

42. Hu, Y.P.; Li, Y.R.; Lu, L.; Mao, Y.J.; Li, M.H. Natural Convection of Water-Based Nanofluids near the Density Maximum in an Annulus. *Int. J. Therm. Sci.* **2020**, *152*, 106309. [CrossRef]

43. Sarafraz, M.M.; Tlili, I.; Tian, Z.; Bakouri, M.; Safaei, M.R.; Goodarzi, M. Thermal Evaluation of Graphene Nanoplatelets Nanofluid in a Fast-Responding HP with the Potential Use in Solar Systems in Smart Cities. *Appl. Sci.* **2019**, *9*, 2101. [CrossRef]

44. Wen, J.; Li, X.; Chen, W.; Liu, J. Systematical Investigation on the Solar-Thermal Conversion Performance of TiN Plasmonic Nanofluids for the Direct Absorption Solar Collectors. *Colloids Surf. A Physicochem. Eng. Asp.* **2021**, *624*, 126837. [CrossRef]

45. Borode, A.; Ahmed, N.; Olubambi, P. A Review of Solar Collectors Using Carbon-Based Nanofluids. *J. Clean. Prod.* **2019**, *241*, 118311. [CrossRef]

46. Said, Z.; Abdelkareem, M.A.; Rezk, H.; Nassef, A.M.; Atwany, H.Z. Stability, Thermophysical and Electrical Properties of Synthesized Carbon Nanofiber and Reduced-Graphene Oxide-Based Nanofluids and Their Hybrid along with Fuzzy Modeling Approach. *Powder Technol.* **2020**, *364*, 795–809. [CrossRef]

47. Taherialekouhi, R.; Rasouli, S.; Khosravi, A. An Experimental Study on Stability and Thermal Conductivity of Water-Graphene Oxide/Aluminum Oxide Nanoparticles as a Cooling Hybrid Nanofluid. *Int. J. Heat Mass Transf.* **2019**, *145*, 118751. [CrossRef]

48. Verma, S.K.; Tiwari, A.K.; Tiwari, S.; Chauhan, D.S. Performance Analysis of Hybrid Nanofluids in Flat Plate Solar Collector as an Advanced Working Fluid. *Sol. Energy* **2018**, *167*, 231–241. [CrossRef]

49. Said, Z.; Sajid, M.H.; Saidur, R.; Mahdiraji, G.A.; Rahim, N.A. Evaluating the Optical Properties of TiO$_2$ Nanofluid for a Direct Absorption Solar Collector. *Numer. Heat Transf. Part A Appl.* **2015**, *67*, 1010–1027. [CrossRef]

50. Howe, M.L.; Paul, T.C.; Khan, J.A. Radiative Properties of Al$_2$O$_3$ Nanoparticles Enhanced Ionic Liquids (NEILs) for Direct Absorption Solar Collectors. *Sol. Energy Mater. Sol. Cells* **2021**, *232*, 111327. [CrossRef]

51. Ambreen, T.; Kim, M.H. Influence of Particle Size on the Effective Thermal Conductivity of Nanofluids: A Critical Review. *Appl. Energy* **2020**, *264*, 114684. [CrossRef]

52. Goshayeshi, H.R.; Safaei, M.R.; Goodarzi, M.; Dahari, M. Particle Size and Type Effects on Heat Transfer Enhancement of Ferro-Nanofluids in a Pulsating Heat Pipe. *Powder Technol.* **2016**, *301*, 1218–1226. [CrossRef]

53. Motevasel, M.; Nazar, A.R.S.; Jamialahmadi, M. The Effect of Nanoparticles Aggregation on the Thermal Conductivity of Nanofluids at Very Low Concentrations: Experimental and Theoretical Evaluations. *Heat Mass Transf. und Stoffuebertragung* **2018**, *54*, 125–133. [CrossRef]

54. Maheshwary, P.B.; Handa, C.C.; Nemade, K.R. A Comprehensive Study of Effect of Concentration, Particle Size and Particle Shape on Thermal Conductivity of Titania/Water Based Nanofluid. *Appl. Therm. Eng.* **2017**, *119*, 79–88. [CrossRef]

55. Nikkam, N.; Ghanbarpour, M.; Khodabandeh, R.; Toprak, M.S. The Effect of Particle Size and Base Liquid on Thermo-Physical Properties of Ethylene and Diethylene Glycol Based Copper Micro- and Nanofluids. *Int. Commun. Heat Mass Transf.* **2017**, *86*, 143–149. [CrossRef]

56. Abbasi, M.; Heyhat, M.M.; Rajabpour, A. Study of the Effects of Particle Shape and Base Fluid Type on Density of Nanofluids Using Ternary Mixture Formula: A Molecular Dynamics Simulation. *J. Mol. Liq.* **2020**, *305*, 112831. [CrossRef]

57. Qin, C.; Kim, J.B.; Gonome, H.; Lee, B.J. Absorption Characteristics of Nanoparticles with Sharp Edges for a Direct-Absorption Solar Collector. *Renew. Energy* **2020**, *145*, 21–28. [CrossRef]

58. Song, D.; Yang, Y.; Jing, D. Insight into the Contribution of Rotating Brownian Motion of Nonspherical Particle to the Thermal Conductivity Enhancement of Nanofluid. *Int. J. Heat Mass Transf.* **2017**, *112*, 61–71. [CrossRef]

59. Bahiraei, M.; Monavari, A.; Moayedi, H. Second Law Assessment of Nanofluid Flow in a Channel Fitted with Conical Ribs for Utilization in Solar Thermal Applications: Effect of Nanoparticle Shape. *Int. J. Heat Mass Transf.* **2020**, *151*, 119387. [CrossRef]

60. Bahiraei, M.; Monavari, A.; Naseri, M.; Moayedi, H. Irreversibility Characteristics of a Modified Microchannel Heat Sink Operated with Nanofluid Considering Different Shapes of Nanoparticles. *Int. J. Heat Mass Transf.* **2020**, *151*, 119359. [CrossRef]

61. Afrand, M. Experimental Study on Thermal Conductivity of Ethylene Glycol Containing Hybrid Nano-Additives and Development of a New Correlation. *Appl. Therm. Eng.* **2017**, *110*, 1111–1119. [CrossRef]

62. Esfahani, N.N.; Toghraie, D.; Afrand, M. A New Correlation for Predicting the Thermal Conductivity of ZnO–Ag (50%–50%)/Water Hybrid Nanofluid: An Experimental Study. *Powder Technol.* **2018**, *323*, 367–373. [CrossRef]

63. Hemmat Esfe, M.; Behbahani, P.M.; Arani, A.A.A.; Sarlak, M.R. Thermal Conductivity Enhancement of SiO₂–MWCNT (85:15%)–EG Hybrid Nanofluids: ANN Designing, Experimental Investigation, Cost Performance and Sensitivity Analysis. *J. Therm. Anal. Calorim.* **2017**, *128*, 249–258. [CrossRef]

64. Shahsavar, A.; Bahiraei, M. Experimental Investigation and Modeling of Thermal Conductivity and Viscosity for Non-Newtonian Hybrid Nanofluid Containing Coated CNT/Fe₃O₄ Nanoparticles. *Powder Technol.* **2017**, *318*, 441–450. [CrossRef]

65. Kannaiyan, S.; Boobalan, C.; Umasankaran, A.; Ravirajan, A.; Sathyan, S.; Thomas, T. Comparison of Experimental and Calculated Thermophysical Properties of Alumina/Cupric Oxide Hybrid Nanofluids. *J. Mol. Liq.* **2017**, *244*, 469–477. [CrossRef]

66. Koca, H.D.; Doganay, S.; Turgut, A.; Tavman, I.H.; Saidur, R.; Mahbubul, I.M. Effect of Particle Size on the Viscosity of Nanofluids: A Review. *Renew. Sustain. Energy Rev.* **2018**, *82*, 1664–1674. [CrossRef]

67. Murshed, S.M.S.; Estellé, P. A State of the Art Review on Viscosity of Nanofluids. *Renew. Sustain. Energy Rev.* **2017**, *76*, 1134–1152. [CrossRef]

68. Motahari, K.; Abdollahi Moghaddam, M.; Moradian, M. Experimental Investigation and Development of New Correlation for Influences of Temperature and Concentration on Dynamic Viscosity of MWCNT-SiO₂ (20–80)/20W50 Hybrid Nano-Lubricant. *Chinese J. Chem. Eng.* **2018**, *26*, 152–158. [CrossRef]

69. Zareie, A.; Akbari, M. Hybrid Nanoparticles Effects on Rheological Behavior of Water-EG Coolant under Different Temperatures: An Experimental Study. *J. Mol. Liq.* **2017**, *230*, 408–414. [CrossRef]

70. Alirezaie, A.; Saedodin, S.; Esfe, M.H.; Rostamian, S.H. Investigation of Rheological Behavior of MWCNT (COOH-Functionalized)/MgO—Engine Oil Hybrid Nanofluids and Modelling the Results with Artificial Neural Networks. *J. Mol. Liq.* **2017**, *241*, 173–181. [CrossRef]

71. Asadi, M.; Asadi, A.; Aberoumand, S. An Experimental and Theoretical Investigation on the Effects of Adding Hybrid Nanoparticles on Heat Transfer Efficiency and Pumping Power of an Oil-Based Nanofluid as a Coolant Fluid. *Int. J. Refrig.* **2018**, *89*, 83–92. [CrossRef]

72. Huminic, G.; Huminic, A. Hybrid Nanofluids for Heat Transfer Applications—A State-of-the-Art Review. *Int. J. Heat Mass Transf.* **2018**, *125*, 82–103. [CrossRef]

73. Sharaf, O.Z.; Al-Khateeb, A.N.; Kyritsis, D.C.; Abu-Nada, E. Four-Way Coupling of Particle-Wall and Colloidal Particle-Particle Interactions in Direct Absorption Solar Collectors. *Energy Convers. Manag.* **2019**, *195*, 7–20. [CrossRef]

74. Sharaf, O.Z.; Al-Khateeb, A.N.; Kyritsis, D.C.; Abu-Nada, E. Numerical Investigation of Nanofluid Particle Migration and Convective Heat Transfer in Microchannels Using an Eulerian–Lagrangian Approach. *J. Fluid Mech.* **2019**, *878*, 62–97. [CrossRef]

75. Sharaf, O.Z.; Al-Khateeb, A.N.; Kyritsis, D.C.; Abu-Nada, E. Energy and Exergy Analysis and Optimization of Low-Flux Direct Absorption Solar Collectors (DASCs): Balancing Power- and Temperature-Gain. *Renew. Energy* **2019**, *133*, 861–872. [CrossRef]

76. Gorji, T.B.; Ranjbar, A.A. Geometry Optimization of a Nanofluid-Based Direct Absorption Solar Collector Using Response Surface Methodology. *Sol. Energy* **2015**, *122*, 314–325. [CrossRef]

77. Vital, C.V.P.; Farooq, S.; de Araujo, R.E.; Rativa, D.; Gómez-Malagón, L.A. Numerical Assessment of Transition Metal Nitrides Nanofluids for Improved Performance of Direct Absorption Solar Collectors. *Appl. Therm. Eng.* **2021**, *190*, 116799. [CrossRef]

78. Struchalin, P.G.; Yunin, V.S.; Kutsenko, K.V.; Nikolaev, O.V.; Vologzhannikova, A.A.; Shevelyova, M.P.; Gorbacheva, O.S.; Balakin, B.V. Performance of a Tubular Direct Absorption Solar Collector with a Carbon-Based Nanofluid. *Int. J. Heat Mass Transf.* **2021**, *179*, 121717. [CrossRef]

79. Struchalin, P.G.; Kuzmenkov, D.M.; Yunin, V.S.; Wang, X.; He, Y.; Balakin, B.V. Hybrid Nanofluid in a Direct Absorption Solar Collector: Magnetite vs. Carbon Nanotubes Compete for Thermal Performance. *Energies* **2022**, *15*, 1604. [CrossRef]

80. Wang, D.; Liang, W.; Zheng, Z.; Jia, P.; Yan, Y.; Xie, H.; Wang, L.; Yu, W. Highly Efficient Energy Harvest via External Rotating Magnetic Field for Oil Based Nanofluid Direct Absorption Solar Collector. *Green Energy Environ.* **2021**, *6*, 298–307. [CrossRef]

81. Hooshmand, A.; Zahmatkesh, I.; Karami, M.; Delfani, S. Porous Foams and Nanofluids for Thermal Performance Improvement of a Direct Absorption Solar Collector: An Experimental Study. *Environ. Prog. Sustain. Energy* **2021**, *40*, e13684. [CrossRef]

82. Zhang, H.; Wang, K.; Yu, W.; Wang, L.; Xie, H. Ternary Molten Salt Energy Storage Coupled with Graphene Oxide-TiN Nanofluids for Direct Absorption Solar Collector. *Energy Build.* **2021**, *253*, 111481. [CrossRef]

83. Peng, W.; Sadaghiani, O.K. Thermal Performance Enhancement of Direct Absorption Solar Collector Using Nanoparticle in Sunray Trap. *Appl. Therm. Eng.* **2021**, *187*, 116578. [CrossRef]

84. Qin, C.; Lee, J.; Lee, B.J. A Hybrid Direct-Absorption Parabolic-Trough Solar Collector Combining Both Volumetric and Surface Absorption. *Appl. Therm. Eng.* **2021**, *185*, 116333. [CrossRef]

85. Kumar, R.; Bharadwaj, G.; Kharub, M.; Goel, V.; Kumar, A. Performance Analysis of Nanofluid Based Direct Absorption Solar Collector of Different Configurations: A Two-Phase CFD Modeling. *Energy Sources Part A Recovery Util. Environ. Eff.* **2022**. [CrossRef]

86. Karami, M.; Somayeh, S.; Gahraz, N. Improving Thermal Performance of a Solar Thermal/Desalination Combisystem Using Nanofluid-Based Direct Absorption Solar Collector. *Sci. Iran.* **2021**, *29*, 1288–1300. [CrossRef]

87. Bhalla, V.; Khullar, V.; Tyagi, H. Investigation of Factors Influencing the Performance of Nanofluid-Based Direct Absorption Solar Collector Using Taguchi Method. *J. Therm. Anal. Calorim.* **2018**, *135*, 1493–1505. [CrossRef]

88. Gorji, T.B.; Ranjbar, A.A. A Numerical and Experimental Investigation on the Performance of a Low-Flux Direct Absorption Solar Collector (DASC) Using Graphite, Magnetite and Silver Nanofluids. *Sol. Energy* **2016**, *135*, 493–505. [CrossRef]

89. Thakur, P.P.; Khapane, T.S.; Sonawane, S.S. Comparative Performance Evaluation of Fly Ash-Based Hybrid Nanofluids in Microchannel-Based Direct Absorption Solar Collector. *J. Therm. Anal. Calorim.* **2021**, *143*, 1713–1726. [CrossRef]

90. Parvin, S.; Nasrin, R.; Alim, M.A. Heat Transfer and Entropy Generation through Nanofluid Filled Direct Absorption Solar Collector. *Int. J. Heat Mass Transf.* **2014**, *71*, 386–395. [CrossRef]

91. Sharaf, O.Z.; Al-Khateeb, A.N.; Kyritsis, D.C.; Abu-Nada, E. Direct Absorption Solar Collector (DASC) Modeling and Simulation Using a Novel Eulerian-Lagrangian Hybrid Approach: Optical, Thermal, and Hydrodynamic Interactions. *Appl. Energy* **2018**, *231*, 1132–1145. [CrossRef]

92. Hazra, S.K.; Michael, M.; Nandi, T.K. Investigations on Optical and Photo-Thermal Conversion Characteristics of BN-EG and BN/CB-EG Hybrid Nanofluids for Applications in Direct Absorption Solar Collectors. *Sol. Energy Mater. Sol. Cells* **2021**, *230*, 111245. [CrossRef]

93. Wang, K.; He, Y.; Zheng, Z.; Gao, J.; Kan, A.; Xie, H.; Yu, W. Experimental Optimization of Nanofluids Based Direct Absorption Solar Collector by Optical Boundary Conditions. *Appl. Therm. Eng.* **2021**, *182*, 116076. [CrossRef]

94. Shen, C.; Yang, Q.; Zhang, C.; Ma, S.; Dong, Y. Optimized Optical Properties of Au Nanorods with Flow Regulation to Enhance the Performance of Direct Absorption Solar Collectors. *Sol. Energy* **2021**, *218*, 611–620. [CrossRef]

95. Zhu, Y.; Li, P.; Ruan, Z.; Yuan, Y. A Model and Thermal Loss Evaluation of a Direct-Absorption Solar Collector under the Influence of Radiation. *Energy Convers. Manag.* **2022**, *251*, 114933. [CrossRef]

96. Sharaf, O.Z.; Kyritsis, D.C.; Abu-Nada, E. Impact of Nanofluids, Radiation Spectrum, and Hydrodynamics on the Performance of Direct Absorption Solar Collectors. *Energy Convers. Manag.* **2018**, *156*, 706–722. [CrossRef]

97. Fang, J.; Xuan, Y. Investigation of Optical Absorption and Photothermal Conversion Characteristics of Binary CuO/ZnO Nanofluids. *RSC Adv.* **2017**, *7*, 56023–56033. [CrossRef]

98. Bhalla, V.; Khullar, V.; Tyagi, H. Experimental Investigation of Photo-Thermal Analysis of Blended Nanoparticles (Al_2O_3/Co_3O_4) for Direct Absorption Solar Thermal Collector. *Renew. Energy* **2018**, *123*, 616–626. [CrossRef]

99. Mehrali, M.; Ghatkesar, M.K.; Pecnik, R. Full-Spectrum Volumetric Solar Thermal Conversion via Graphene/Silver Hybrid Plasmonic Nanofluids. *Appl. Energy* **2018**, *224*, 103–115. [CrossRef]

100. Qu, J.; Zhang, R.; Wang, Z.; Wang, Q. Photo-Thermal Conversion Properties of Hybrid CuO-MWCNT/H_2O Nanofluids for Direct Solar Thermal Energy Harvest. *Appl. Therm. Eng.* **2019**, *147*, 390–398. [CrossRef]

101. Khashan, S.; Dagher, S.; Al Omari, S.; Tit, N.; Elnajjar, E.; Mathew, B.; Hilal-Alnaqbi, A. Photo-Thermal Characteristics of Water-Based $Fe_3O_4@SiO_2$ Nanofluid for Solar-Thermal Applications. *Mater. Res. Express* **2017**, *4*, 055701. [CrossRef]

102. Zeiny, A.; Jin, H.; Bai, L.; Lin, G.; Wen, D. A Comparative Study of Direct Absorption Nanofluids for Solar Thermal Applications. *Sol. Energy* **2018**, *161*, 74–82. [CrossRef]

103. Karami, M. Experimental Investigation of First and Second Laws in a Direct Absorption Solar Collector Using Hybrid Fe_3O_4/SiO_2 Nanofluid. *J. Therm. Anal. Calorim.* **2019**, *136*, 661–671. [CrossRef]

104. Wang, X.; He, Y.; Chen, M.; Hu, Y. ZnO-Au Composite Hierarchical Particles Dispersed Oil-Based Nanofluids for Direct Absorption Solar Collectors. *Sol. Energy Mater. Sol. Cells* **2018**, *179*, 185–193. [CrossRef]

105. Sharaf, O.Z.; Kyritsis, D.C.; Al-Khateeb, A.N.; Abu-Nada, E. Effect of Bottom Surface Optical Boundary Conditions on Nanofluid-Based DASC: Parametric Study and Optimization. *Sol. Energy* **2018**, *164*, 210–223. [CrossRef]

106. Karami, M.; Bozorgi, M.; Delfani, S.; Akhavan-Behabadi, M.A. Empirical Correlations for Heat Transfer in a Silver Nanofluid-Based Direct Absorption Solar Collector. *Sustain. Energy Technol. Assessments* **2018**, *28*, 14–21. [CrossRef]